Determination of the effective transverse coherence of the neutron wave packet as employed in reflectivity investigations of condensed-matter structures. II. Analysis of elastic scattering using energy-gated wave packets with an application to neutron reflection from ruled gratings

N. F. Berk

NIST Center for Neutron Scattering, National Institute of Standards and Technology, Gaithersburg, Maryland 20899, USA
and Department of Materials Science and Engineering, University of Maryland, College Park, Maryland 20742, USA

(Received 6 September 2013; published 27 March 2014)

We present a general approach to analyzing elastic scattering for those situations where the incident beam is prepared as an incoherent ensemble of wave packets of a given arbitrary shape. Although wave packets, in general, are not stationary solutions of the Schrödinger equation, the analysis of elastic scattering data treats the scattering as a stationary-state problem. We thus must *gate* the wave packet, coherently distorting its shape in a manner consistent with the elastic condition. The resulting gated scattering amplitudes (e.g., reflection coefficients) thus are weighted *coherent* sums of the constituent plane-wave scattering amplitudes, with the weights determined by the shape of the incident wave packet as "filtered" by energy gating. We develop the gating formalism in general and apply it to the problem of neutron scattering from ruled gratings described by Majkrzak *et al*. in a companion paper. The required exact solution of the associated problem of plane-wave reflection from gratings also is derived.

DOI: 10.1103/PhysRevA.89.033852 PACS number(s): 42.25.Kb, 61.05.fm, 03.75.Dg, 61.05.fj

I. INTRODUCTION

In this paper we address the problem of analyzing elastic scattering, especially as in reflectometry, when the incident wave (for a single incident quantum of radiation) is a shaped wave packet poorly approximated by a perfect plane wave. The basic idea is simple enough: The incident wave packet is in general a solution of the time-dependent Schrödinger equation, but standard analysis of data treats the elastic scattering as a stationary-state problem, thereby effectively *gating* the wave packet, i.e., distorting its shape in a manner consistent with the elastic condition. The resulting gated scattering amplitudes (e.g., reflection coefficients) thus are weighted *coherent* sums of the constituent plane-wave scattering amplitudes, with the weights determined by the shape of the incident wave packet as "filtered" by energy gating. Among its benefits, gated analysis leads to well-defined notions of longitudinal and transverse "coherence lengths" and their effects on the scattering, which usually are treated rather phenomenologically. The price paid for gated wave-packet analysis is the need of an accurate description of the underlying perfect plane-wave scattering, especially in the dynamical regime, where the Born approximation fails. Our notion of the energy-gated wave packet was motivated in part by the approach of Zhu *et al*. [1] to the problem of defining a time-independent Lippmann-Schwinger description of wave-packet scattering. The formulation of wave-packet scattering described here was applied to the analysis of neutron scattering from ruled gratings in a companion paper by Majkrzak *et al*. [2], hereafter referred to as Part I.

In this work the wave packet of study is taken as the complete description of the quantum mechanical state of a single particle—say, a neutron—in the physical space of the scattering and detection events. No account is taken of the source of the incident particles, but each particle is viewed as being totally uncorrelated with any other, as appropriate for the description of an incoherent incident beam of like particles, as produced, say, in the core of a nuclear reactor. However, no explicit consideration is given to the processes responsible for the assumed shape of the wave packet, which, for neutrons, may include interactions with moderators, filters, guide tubes, collimators, monochromators, and so on. We also assume a "perfect instrument" once the particle is in the incident field of the sample, and we neglect postscattering effects related to slit settings and detector characteristics. For our purposes, such matters lie within the realm of the usual incoherent instrumental effects which act to select or reject particles either from being incident upon the sample or from being detected after scattering. See Part I for a discussion of instrumental considerations and for an analysis of relevant "upstream" effects that could influence wave-packet shape for a neutron beam or which may even be connected to imperfections in the sample itself, thus acting to partially mask the coherent behavior of the single-particle wave packet.

In Sec. II we derive the gated wave-packet formalism in some generality in the context of neutron reflectivity, taking up a number of implementation matters in Sec. III. The theory is developed first for specular-only reflection in Sec. III A and for nonspecular reflection in Sec. III B, and a definition of observable reflection amplitudes is shown in Eq. (54b). The concept of coherent aliasing, or misidentification of scattered rays, is introduced in Sec. IV. The application to ruled gratings, the subject of Part I of this work, is described in Sec. IV. The Appendix presents an exact formulation of plane-wave scattering from ruled gratings using a Green's function technique, which was used in the gated wave-packet analysis of data in Part I.

A general discussion of wave packets may be found in the textbook by Tannor [3], while copious theoretical material specific to neutron scattering is in the handbook by Utsoro and Ignatovich [4]. Treatments of dynamical plane-wave neutron scattering from gratings have also been developed by Tolan *et al*. [5] and by Ashkar *et al*. [6]. References relating to wave-packet scattering in a variety of contexts, both theoretical and experimental, are listed in Part I.

Before moving on to the problem at hand, it is worthwhile emphasizing that while the gated wave-packet notion may seem intuitive enough, it constitutes a particular approach to the analysis of neutron scattering in its traditional setting. Its essential idea is to make a sharp distinction between the totally coherent superposition of momentum eigenstates implicit in any wave packet fully describing a single incident neutron—thus resulting in a coherent superposition of virtual plane-wave incident angles—and the incoherent distribution of energy and momentum eigenstates associated with the ensemble of different neutrons in the incident beam, however realized in a particular instrumental setup. As discussed in detail in Secs. I and II of Part I, this separation of coherent from incoherent behavior of typical neutron beams stems from the overtly incoherent generation of particles, be it by nuclear fission or spallation. Such partitioning of coherent from incoherent character of the beam does not apply, in general, to all radiation sources, light sources especially. Thus, all treatments of wave-packet scattering cannot be assumed to be universally applicable, and it follows that all approaches that have been discussed over time for quantifying beam correlation lengths and related properties (many of these cited in Part I) are not necessarily appropriate to a chosen problem of interest.

The remaining point is why, specifically, we need wave-packet energy gating. The underlying mathematical problem originates in the fact that, as mentioned earlier, we normally analyze elastic neutron scattering with stationary-state formalism, as if it were scattering of monoenergetic plane waves. The scattering data thus are characterized in terms of sharply defined incident and scattered momenta and resulting momentum transfers (setting aside instrumental resolution). Wave packets, however, are not stationary solutions of the time-dependent Schrödinger equation and thus the collection and refinement of data as if they were requires a formalism distinct in principle from that associated with the usual assumptions. In more technical terms, the equivalence of the time-dependent Schrödinger equation and the time-independent Lippmann-Schwinger (LS) equation only holds for stationary solutions of the former, and it is the latter equation that gives us explicit and exact formulas for scattering amplitudes in terms of the scattering potential and these solutions. In Zhu *et al*. [1] energy gating (they do not use this terminology) leads to an exact, modified version of the LS equation. As we see below, this fact, combined with the energy gating implicit in conventional analysis of scattering, allows us, employing different methods, to maintain the fundamental relationships between scattered waves and the scattering potential—perfectly well defined for plane-wave scattering—but now folded into what might be called the "coherent collimation" intrinsic to the gated wave packet. From this perspective one may view the energy-gated wave-packet formalism as the primary elastic scattering theory for neutrons. Because plane waves, by mathematical definition, have infinite spatial extent, the very notion of the physical separation of incident from scattered waves presents conceptual difficulties that are generally overlooked in applications of the stationary-state scattering paradigm or which are handled, as it were, by "thinking" wave packets while "doing" plane waves. However, in energy-gated wave-packet theory, to be introduced in Sec. II B in the context of neutron reflection, the exact (dynamical) stationary solutions are not taken as physical entities (except for satisfying required boundary conditions); they appear instead as appropriate basis states in which to represent the energy-gated physical solutions of the time-dependent Schrödinger equation. Thus, the physical realization (i.e., observation) of dynamical plane-wave scattering itself emerges asymptotically from energy-gated wave-packet theory in the limit that the wave packets are sufficiently delocalized with respect to the germane spatial properties of the scattering sample and the surrounding apparatus. Fortunately, this limit has proven to be appropriate—or at least adequate—for a wide range of problems in neutron scattering; but experiments on large-period gratings described in Part I show that the gated wave packet is itself rendered observable by its coherent interplay with the various relevant spatial scales in the experimental setup. Therefore, as a matter of principle, the more comprehensive theory is called for.

In Sec. V, following the mathematical development, we return to a brief summary of these major points along with a few additional concluding remarks.

II. GATED WAVE PACKETS

A. Preliminaries

In order to facilitate a mathematical analysis of the reflection problem we assume a "slab" topology in which the relevant space of the scattering problem is partitioned into three regions having planar boundaries parallel to the surface of the sample (film) slab. Taking the z axis along an inward normal to the film, these regions are I, $z < 0$, the space above (in front of) the film, containing the incident and reflected waves; II, $0 \leqslant z < L$, containing the film of thickness L; and III, $z \geqslant L$, the space below (behind) the film, containing a substrate (if required) and the transmitted wave. Since we are dealing with a three-dimensional problem, it is also useful to think of region I as having "incidence" and "reflection" subspaces, $\mathrm{I_i}$ and $\mathrm{I_r}$; then the wave packet fully describing a single incident neutron is prepared somewhere in $\mathrm{I_i}$, while the reflected wave packet is detected in $\mathrm{I_r}$. Similarly, the transmitted wave packet is detected in $\mathrm{III_t}$. It also will be helpful to to define the subspace where the scattered wave packet, either reflected or transmitted, is detected as $\Omega_d = \mathrm{I_r} \bigcup \mathrm{III_t}$.

Clearly, even at this rudimentary level of description we cannot easily envision "incident" and "scattered" plane waves without some attendant notion of localization. A common conception is to interpret plane waves in this context as describing "beams of particles" that we conveniently may view as localized when it suits the picture of scattering by billiard balls or the like. Our view, as laid out in Sec. I, is that the individual incident neutrons in the beam act independently and are physically localized to an extent limiting how they can *coherently* interact with the film of interest (or any part of the measuring apparatus). From this perspective, "perfect plane waves" are a convenient basis in the Hilbert space of the problem of individual scattering events, since wave packets can be analyzed as coherent superpositions of plane waves—or, as we do below—as superpositions of exact representations of plane-wave scattering. That single plane waves usually give an accurate description of scattering follows, in this picture,

from the fact that, fortunately, wave packets that are not too well localized on the scale of the relevant geometry of the scatterer do behave (mathematically) more or less as perfect plane waves.

B. Wave-packet scattering

Now let $\psi(\mathbf{r},t)$, for $t \geqslant t_0$, be the exact solution of the scattering problem for an incident wave packet defined by its initial form $\psi(\mathbf{r},t_0)$, which we assume is entirely supported in a region $\mathbf{r} \in \mathrm{I}_0 \subset \mathrm{I}_\mathrm{i}$. It is natural—and usually justified—to think of the subspaces identified with wave-packet "preparation" and "detection" as being well separated, such that $\mathrm{I}_0 \bigcap \Omega_\mathrm{d} \approx 0$. In what follows we refer to this as the *separation* assumption and call the more stringent $\mathrm{I}_0 \bigcap \Omega_\mathrm{d} = 0$ the *strong separation* condition.

$\psi(\mathbf{r},t)$ satisfies the time-dependent Schrödinger equation (TDSE),

$$H\psi = i\hbar\partial_t\psi, \tag{1}$$

where $H = -\frac{\hbar^2}{2m}\nabla^2 + U(\mathbf{r}) = K + U$ and U is the film potential in II, which—for t-independent H—has the formal, energy-conserving (elastic scattering) solution

$$\psi(t) = e^{-iH(t-t_0)/\hbar}\psi(t_0). \tag{2}$$

(We sometimes suppress arguments.) This defines $\psi(t)$ at all t, but given that $\psi(t_0)$ is known—i.e., has been prepared in region I_0—we are only interested in $\psi(,t)$ for $t > t_0$. Since $H = K$ in region I, the TDSE has stationary solutions,

$$\psi_\mathbf{k}(\mathbf{r},t) = e^{-iE_\mathbf{k}/\hbar t}\psi_\mathbf{k}(\mathbf{r}), \tag{3}$$

corresponding to incident plane waves $e^{i\mathbf{k}\cdot\mathbf{r}}$ with $E_\mathbf{k} = \hbar^2k^2/2m = \hbar\omega_\mathbf{k}$, where $\psi_k(\mathbf{r})$ satisfies the time-independent Schrödinger equation (TISE),

$$H\psi(\mathbf{r}) = E_\mathbf{k}\psi_\mathbf{k}(\mathbf{r}). \tag{4}$$

We take the $\psi_\mathbf{k}$ to be the unique "physical" solutions of (4), i.e., the solutions satisfying boundary conditions appropriate to the scattering experiment defined earlier: incident wave in region I_i, reflected wave in I_r and transmitted wave in III_t. These time-independent states are eigenfunctions of the Hermitian operator H and thus, in D spatial dimensions, form a complete orthonormal basis for the scattering problem,

$$\int \psi^*_{\mathbf{k}'}(\mathbf{r})\psi_\mathbf{k}(\mathbf{r})\,d^Dr = \frac{(2\pi)^D}{V}\delta(\mathbf{k}'-\mathbf{k}) \tag{5a}$$

and

$$\frac{V}{(2\pi)^D}\int \psi^*_\mathbf{k}(\mathbf{r}')\psi_\mathbf{k}(\mathbf{r})\,d^Dk = \delta(\mathbf{r}'-\mathbf{r}). \tag{5b}$$

The general concerns at hand require $D = 3$, of course, but for $U(\mathbf{r})$ which vary over fewer dimensions, the effective dimension of the scattering problem can be reduced to $D = 2$ or even $D = 1$, as in specular reflection from a perfectly smooth film. As is well known, normalization and completeness are technically delicate matters in the scattering theory, because states are labeled by a continuous "quantum" number $\mathbf{k}$ and true plane waves are not normalizable; they do not quite "fit" into a separable Hilbert space, unless it is *rigged* to accept them, which we take for granted (e.g., see [7], Sec. 1.4). The multiplier of the Dirac δ function in (5a) accounts for "box normalization" of plane waves and is required for dimensional consistency; $\psi_\mathbf{k}(\mathbf{r}) \to e^{i\mathbf{k}\cdot\mathbf{r}}/\sqrt{V}$, where V is the volume of the scattering setup, with the limit $V \to \infty$ understood. The "value" of $\delta(\mathbf{k}'-\mathbf{k})/V$ can be thought of, casually, as unity for $\mathbf{k}'$ within a d^Dk neighborhood of $\mathbf{k}$. Thus, scattering states are normalized here to $(2\pi)^D$. The factor $(2\pi)^D$ is required by the integral representation of the δ function,

$$\int_\infty e^{i\mathbf{k}\cdot\mathbf{r}}\,d^Dr = (2\pi)^D\delta(\mathbf{r}),$$

where

$$\int_\infty \cdots d^Du = \int_{-\infty}^{\infty}\cdots\int_{-\infty}^{\infty} du_1\cdots du_D,$$

for any D-dimensional $\mathbf{u}$. (We usually write the limits explicitly for $D = 1$ to avoid possible confusion.) The similar prefactor in (5b) expresses the conversion of a sum to an integral:

$$\sum_{\mathbf{k}_n}\cdots \to \frac{V}{(2\pi)^D}\int_\infty \cdots d^Dk.$$

[It is common to define $\psi_\mathbf{k}(\mathbf{r}) \to e^{i\mathbf{k}\cdot\mathbf{r}}/\sqrt{(2\pi)^DV}$ for normalization to unity.] Consistent with the form of the stationary plane-wave state,

$$\psi_\mathbf{k}(\mathbf{r}) = e^{i\mathbf{k}\cdot\mathbf{r}}e^{-i\omega_\mathbf{k}t}, \tag{6}$$

the Fourier transform $\tilde{f}(\mathbf{k},\omega)$ of a function $f(\mathbf{r},t)$ is defined here as

$$\tilde{f}(\mathbf{k},\omega) = \int_\infty\int_{-\infty}^{\infty} e^{-i\mathbf{k}\cdot\mathbf{r}}e^{i\omega t}f(\mathbf{r},t)\,d^Dr\,dt,$$

with the inverse transform

$$f(\mathbf{k},\omega) = \int_\infty\int_{-\infty}^{\infty} e^{i\mathbf{k}\cdot\mathbf{r}}e^{-i\omega t}\tilde{f}(\mathbf{k},\omega)\,\frac{d^Dk}{(2\pi)^D}\,\frac{d\omega}{2\pi}.$$

According to Plancherel's theorem, the existence of either integral implies the existence of the other. From here on, we follow the convention of setting $V = 1$ in (5), so that plane-wave states can be represented simply as $\psi_\mathbf{k}(\mathbf{r}) \to e^{i\mathbf{k}\cdot\mathbf{r}}$, which leads to more transparent looking equations than otherwise. Strictly speaking, this entails rescaling $\mathbf{r}$ and $\mathbf{k}$, but we not need to worry about this for now.

The initial state, i.e., the prepared wave packet $\psi(\mathbf{r},t_0)$, can be expanded in the stationary-state basis as

$$\psi(\mathbf{r},t_0) = \int A_\mathbf{k}\psi_\mathbf{k}(\mathbf{r})\,\frac{d^Dk}{(2\pi)^D}, \tag{7a}$$

where, from (5a),

$$A_\mathbf{k} = \int \psi^*_\mathbf{k}(\mathbf{r})\psi(\mathbf{r},t_0)\,d^Dr. \tag{7b}$$

Now write

$$\psi_\mathbf{k}(\mathbf{r}) = e^{i\mathbf{k}\cdot\mathbf{r}} + \psi^s_\mathbf{k}(\mathbf{r}), \tag{8}$$

where $\psi^s_\mathbf{k}(\mathbf{r})$ is the scattered basis component for incident $e^{i\mathbf{k}\cdot\mathbf{r}}$. This scattered wave effectively is *defined* by (8) as $\psi^s_\mathbf{k}(\mathbf{r}) = \psi_\mathbf{k}(\mathbf{r}) - e^{i\mathbf{k}\cdot\mathbf{r}}$, viz., as as component of $\psi^s_\mathbf{k}(\mathbf{r})$ that depends on the presence of nonzero U in region II. The scattered basis

wave thus can exist in regions I, II, and III but is *detected* in what we have defined as Ω_d. Since plane-wave states $e^{i\mathbf{k}\cdot\mathbf{r}}$ also comprise a complete orthonormal set in a rigged Hilbert space, the scattered basis part has an expansion as

$$\psi^s_{\mathbf{k}}(\mathbf{r}) = \int B^s_{\mathbf{k},\mathbf{k}'} e^{i\mathbf{k}'\cdot\mathbf{r}} \frac{d^D k'}{(2\pi)^D}. \tag{9}$$

Then, from (7b) it follows that

$$A_{\mathbf{k}} = A^{(0)}_{\mathbf{k}} + \int B^s_{\mathbf{k},\mathbf{k}'} A^{(0)}_{\mathbf{k}'} \frac{d^D k'}{(2\pi)^D}, \tag{10}$$

where

$$A^{(0)}_{\mathbf{k}} = \int e^{-i\mathbf{k}\cdot\mathbf{r}} \psi(\mathbf{r},t_0)\, d^D r. \tag{11}$$

In the integral part of (10), $A^{(0)}_{\mathbf{k}'}$ delimits the domain of contributing $\mathbf{k}'$ to the set $S^{(0)}_{\mathbf{k}'}$ that defines an incident wave packet, while $B^s_{\mathbf{k},\mathbf{k}'}$ delimits the domain of contributing $\mathbf{k}'$ to the set $S^s_{\mathbf{k},\mathbf{k}'}$ defining scattered plane waves. Assuming that region I_0 is well separated from regions I_r and III, $S^{(0)}_{\mathbf{k}'}$ and $B^s_{\mathbf{k},\mathbf{k}'}$ will tend to have small intersection, leading to $A_{\mathbf{k}} \approx A^{(0)}_{\mathbf{k}}$.

Equations (2), (3), and (7a) lead directly to

$$\psi(\mathbf{r},t) = \int e^{-iE_{\mathbf{k}}(t-t_0)/\hbar} A_{\mathbf{k}} \psi_{\mathbf{k}}(\mathbf{r}) \frac{d^D k}{(2\pi)^D} \tag{12}$$

for the exact evolution of $\psi(\mathbf{r},t)$, where all the information about the incident state preparation is in $A_{\mathbf{k}}$. At this point $A_{\mathbf{k}}$ can be considered to be relatively unrestricted, except that it should describe a wave packet $\psi(\mathbf{r},t)$ that for some period of time $t > t_0$ actually moves toward the film.

Now *define* the function

$$\psi(\mathbf{r},E) \stackrel{\text{def}}{=} \int_{-\infty}^{\infty} e^{iE(t-t_0)/\hbar} \psi(\mathbf{r},t)\, dt, \tag{13}$$

viz., the Fourier transform of $\psi(\mathbf{r},t)$ with respect to t. Then, with the representation of $\psi(\mathbf{r},t)$ from (12), we get

$$\begin{aligned}\psi(\mathbf{r},E) &= \int d^3k\, A_{\mathbf{k}} \psi_{\mathbf{k}}(\mathbf{r}) \int_{-\infty}^{\infty} e^{i(E-E_{\mathbf{k}})(t-t_0)/\hbar}\, dt \\ &= 2\pi\hbar \int A_{\mathbf{k}} \psi_{\mathbf{k}}(\mathbf{r}) \delta(E-E_{\mathbf{k}}) \frac{d^D k}{(2\pi)^D}.\end{aligned} \tag{14}$$

It is easy to see that $\psi(\mathbf{r},E)$ is an eigenstate of H belonging to eigenvalue E:

$$\begin{aligned}H\psi(\mathbf{r},E) &= 2\pi\hbar \int A_{\mathbf{k}} [H\psi_{\mathbf{k}}(\mathbf{r})] \delta(E-E_{\mathbf{k}}) \frac{d^D k}{(2\pi)^D} \\ &= 2\pi\hbar \int A_{\mathbf{k}} [E_{\mathbf{k}}\psi_{\mathbf{k}}(\mathbf{r})] \delta(E-E_{\mathbf{k}}) \frac{d^D k}{(2\pi)^D} \\ &= E\psi(\mathbf{r},E).\end{aligned} \tag{15}$$

Thus, $\psi(\mathbf{r},E)$ is the time-independent component of a stationary state, $\psi(\mathbf{r},E)e^{-iE_{\mathbf{k}}/\hbar t}$. The Dirac δ function in (14) reduces to

$$\delta(E-E_{\mathbf{k}}) = \frac{m}{\hbar^2 k(E)} \delta(k-k(E)),$$

where $k(E) = \sqrt{2mE}/\hbar$. Writing $\mathbf{k} = k\hat{\mathbf{k}}$, the δ function fixes $k = |\mathbf{k}| = k(E)$, leaving only the direction $\hat{\mathbf{k}}$ to integrate over. Therefore, with $d^D k = k^{D-1}\, dk\, d^{D-1}\omega_{\mathbf{k}}$, where the differential solid angle at $\mathbf{k}$, $d^{D-1}\omega_{\mathbf{k}}$, denotes integration over the $D-1$ sphere—i.e., "over the direction of $\mathbf{k}$"—(14) becomes

$$\psi(\mathbf{r},E) = \frac{2\pi m k(E)^{D-2}}{\hbar} \int A_{k(E)\hat{\mathbf{k}}} \psi_{k(E)\hat{\mathbf{k}}}(\mathbf{r}) \frac{d^{D-1}\omega_{\mathbf{k}}}{(2\pi)^D}. \tag{16}$$

Here $\omega_{\mathbf{k}}$, now denoting solid angle, should not be confused with its previous connection to time-dependent analysis, since we are done with that aspect of the development. In standard curvilinear coordinates,

$$d^{D-1}\omega_{\mathbf{k}} = \begin{cases} d\theta, & D=2, \quad \text{polar coordinates,} \\ \sin\theta\, d\theta d\phi, & D=3, \quad \text{spherical coordinates.} \end{cases}$$

For $D=1$ only two points, $\mathbf{k} = \pm k$, comprise the $D-1=0$ sphere; and for this case, we can use polar coordinates for $d^{D-1}\omega_{\mathbf{k}}$ by including the factor $[\delta(\theta)+\delta(\theta-\pi)]$. (This usage of θ and ϕ is only for illustration with conventional notation; below, we use these symbols differently.)

The result in (16) is made more transparent by defining $\Psi_k(\mathbf{r}) = \psi(\mathbf{r},E_{\mathbf{k}})$ and using the identity $k(E_{\mathbf{k}}) = k$. Then

$$\Psi_k(\mathbf{r}) = \frac{2\pi m k^{D-2}}{\hbar} \int A_{\mathbf{k}} \psi_{\mathbf{k}}(\mathbf{r}) \frac{d^{D-1}\omega_{\mathbf{k}}}{(2\pi)^D}. \tag{17}$$

With the substitution of (8) for $\psi_{\mathbf{k}}(\mathbf{r})$, this also can be written as

$$\Psi_k(\mathbf{r}) = \tilde{\psi}^i_k(\mathbf{r}) + \tilde{\psi}^s_k(\mathbf{r}), \tag{18}$$

where

$$\begin{aligned}\tilde{\psi}^i_k(\mathbf{r}) &= \frac{2\pi m k^{D-2}}{\hbar} \int A_{\mathbf{k}} e^{i\mathbf{k}\cdot\mathbf{r}} \frac{d^{D-1}\omega_{\mathbf{k}}}{(2\pi)^D} \\ &\approx \int \psi_{\mathbf{k}}(\mathbf{r},t_0)\delta(E-E_{\mathbf{k}}),\end{aligned} \tag{19a}$$

and

$$\begin{aligned}\tilde{\psi}^r_k(\mathbf{r}) &= \frac{2\pi m k^{D-2}}{\hbar} \int A_{\mathbf{k}} \psi^s_{\mathbf{k}}(\mathbf{r}) \frac{d^{D-1}\omega_{\mathbf{k}}}{(2\pi)^D} \\ &= \int A_{\mathbf{k}} \psi^s_{\mathbf{k}}(\mathbf{r},t_0)\delta(E-E_{\mathbf{k}}) \frac{d^D k}{(2\pi)^D}.\end{aligned} \tag{19b}$$

The "$\approx$" sign is appropriate in (19a) because of (10) and the separation assumption, but with strong separation it can be replaced with "=". Thus, assuming strong separation, (18) behaves as

$$\Psi_k(\mathbf{r}) = \begin{cases} \tilde{\psi}^i_k(\mathbf{r}) & \text{for } \mathbf{r} \in \mathrm{I}_0, \\ \tilde{\psi}^s_k(\mathbf{r}) & \text{otherwise.} \end{cases} \tag{20}$$

For $D=1$ (where $d^0\omega_{\mathbf{k}}$ means evaluate the integrand at $\pm\hat{\mathbf{k}}$ along, say, the z axis),

$$\begin{aligned}\Psi_k(z) &= \frac{2\pi m}{\hbar k}[A_k\psi_k(z) + A_{-k}\psi_{-k}(z)] \\ &= \frac{2\pi m}{\hbar k} A_k \psi_k(z),\end{aligned} \tag{21}$$

if we also define $A(-k) = 0$ for $k > 0$. Except for the 2π, this is Eq. (18) of [1], which considered only one dimension and

used a different tack, although the general approach developed here was mentioned in passing as an alternative. Because of the time integration in (13), $\Psi_k(\mathbf{r})$ depends on t_0 only implicitly in the sense of (7b), which defines $A_\mathbf{k}$ at $t = t_0$. As long as region I_0 is far-enough removed from II, and to the extent we can ignore the spreading of $\psi(\mathbf{r},t_0)$, $\Psi_k(\mathbf{r})$ effectively is independent of t_0. In the special case that $A_\mathbf{k} = \delta(\mathbf{k} - \mathbf{k}_0)$, (17) degenerates to

$$\Psi_k(\mathbf{r}) = \Psi_{k_0}(\mathbf{r}) = \frac{2\pi m k_0^{D-2}}{\hbar}\psi_{\mathbf{k}_0}(\mathbf{r}), \tag{22}$$

which, as expected, is uninformative.

In brief summary, the temporal Fourier transform of $\psi(\mathbf{r},t)$ for an incident wave packet of arbitrary shape in D dimensions produces the function $\psi(\mathbf{r},E) = \Psi_k(\mathbf{r})$, which selects the Fourier content $A_\mathbf{k}$ of the of the incident wave packet $\psi(\mathbf{r},t_0)$ that intersects the $D-1$ sphere of radius $k(E)$ in reciprocal space for any specified energy E. We call $\Psi_k(\mathbf{r})$ the *energy-gated* (or, simply, gated) image of $\psi(\mathbf{r},t)$. In general, wave packets of arbitrary shape are not stationary states of the Schrödinger equation. However, passing $\psi(\mathbf{r},t)$ through a gate that *coherently* discriminates for energy E gives a stationary state $\Psi_k(\mathbf{r})$ uniquely associated with the prepared wave packet $\psi(\mathbf{r},t_0)$. These gated wave packets should properly describe elastic scattering measurements.

Past and future temporal properties of gating

Now one can ask, why not define energy gating only in terms of the wave packet for $t > t_0$, i.e., the "future" behavior of $\psi(\mathbf{r},t_0)$? To answer this, start with the decomposition of (13) into backward- and forward-looking Laplace transforms, viz.,

$$\psi(\mathbf{r},E) = \chi_-(\mathbf{r},E) + \chi_+(\mathbf{r},E), \tag{23}$$

where

$$\chi_-(\mathbf{r},E) = \int_{-\infty}^{t_0} e^{iE(t-t_0)/\hbar}\psi(\mathbf{r},t)\,dt \tag{24a}$$

and

$$\chi_+(\mathbf{r},E) = \int_{t_0}^{\infty} e^{iE(t-t_0)/\hbar}\psi(\mathbf{r},t)\,dt. \tag{24b}$$

Then, using the formula

$$\int_0^\infty e^{i\omega t}\,dt = \int_{-\infty}^0 e^{-i\omega t}\,dt = \pi\delta(\omega) + \frac{i}{\omega}, \tag{25}$$

and (12), the χ's become

$$\chi_\pm(\mathbf{r},E) = \frac{1}{2}\psi(\mathbf{r},E) \pm i\hbar\mathrm{P.P.}\int \frac{A_\mathbf{k}\psi_\mathbf{k}(\mathbf{r})}{E - E_\mathbf{k}}\frac{d^Dk}{(2\pi)^D}, \tag{26}$$

where P.P. denotes the principle part. So

$$\begin{aligned} H\chi_\pm(\mathbf{r},E) &= \frac{1}{2}E\psi(\mathbf{r},E) \pm i\hbar\mathrm{P.P.}\int \frac{A_\mathbf{k}[E_\mathbf{k}\psi_\mathbf{k}(\mathbf{r})]}{E - E_\mathbf{k}}\frac{d^Dk}{(2\pi)^D} \\ &= \frac{1}{2}E\psi(\mathbf{r},E) \pm i\hbar\mathrm{P.P.}\int \frac{A_\mathbf{k}(E_\mathbf{k} - E + E)\psi_\mathbf{k}(\mathbf{r})}{E - E_\mathbf{k}} \\ &\quad\times \frac{d^Dk}{(2\pi)^D} \\ &= E\chi_\pm(\mathbf{r},E) \mp i\hbar\int A_\mathbf{k}\psi_\mathbf{k}(\mathbf{r})\frac{d^Dk}{(2\pi)^D} \\ &= E\chi_\pm(\mathbf{r},E) \mp i\hbar\psi_\mathbf{k}(\mathbf{r},t_0), \end{aligned} \tag{27}$$

using (7a). This result also follows from the definitions in (24) by using (1) under the time integral and integrating by parts, assuming, as usual, that the integrands go to zero as $t \to \infty$. Thus, unlike $\psi(\mathbf{r},E)$ proper, its temporally delimited—past and future—*components* $\chi_\pm(\mathbf{r},E)$ do not separately satisfy the TISE. On the other hand, for $\mathbf{r}$ far from I_0—and for $\psi_\mathbf{k}(\mathbf{r},t_0)$ sufficiently localized in $\mathbf{r} \in \mathrm{I}_0$—(27) gives $H\chi_+(\mathbf{r},E) \approx E\chi_+(\mathbf{r},E)$; i.e., $\chi_+(\mathbf{r},E)$ effectively behaves as a stationary state for $\mathbf{r} \notin \mathrm{I}_0$. Similarly, one can argue that $\chi_-(\mathbf{r},E) \approx 0$ under the same circumstances, since it is defined by the backward propagation of the initial wave packet. In short, with strong separation, (23) infers the asymptotic result

$$\psi(\mathbf{r},E) \sim \chi_+(\mathbf{r},E), \tag{28}$$

i.e., that

$$i\mathrm{P.P.}\int \frac{A_\mathbf{k}\psi_\mathbf{k}(\mathbf{r})}{E - E_\mathbf{k}}\frac{d^Dk}{(2\pi)^D} \sim \frac{1}{2}\psi(\mathbf{r},E) \tag{29}$$

for $\mathbf{r} \notin \mathrm{I}_0$. Since it is much more convenient to compute and analyze the Fourier transform of the exact wave function rather than its forward-looking Laplace transform, it is sensible to define gating this way without introducing serious side effects, as long as strong separation holds.

III. IMPLEMENTATION I: BASIC IDEAS

We look next at the scattered gated wave packet shown in (19b), that is,

$$\tilde{\psi}_k^s(\mathbf{r}) = \frac{2\pi m k^{D-2}}{\hbar}\int A_\mathbf{k}\psi_\mathbf{k}^s(\mathbf{r})\frac{d^{D-1}\omega_\mathbf{k}}{(2\pi)^D}. \tag{30}$$

Recall that under the integral sign, $\psi_\mathbf{k}^s(\mathbf{r})$ is the exact scattered part of the wave function for the perfect plane-wave problem, assumed to have been solved. For the gated problem we first define two coordinate systems. The film space is the one defined in Sec. II A, with the z axis being along an inward normal to the film surface at $z = 0$, the plane separating regions I and II. The film surface thus lies in the x-y plane; we call the coordinate system for the film the II frame. For ease of discussion—and implementation—we reduce the three-dimensional problem to two dimensions, which we take as the z-x plane (we use cyclic ordering in referring to the axes). The reduction to $D = 2$ actually is appropriate for films whose scattering length density varies laterally along a single direction, e.g., a ruled grating, which we consider below in detail. For the purpose of describing the (now two-dimensional) incident wave packet, we use a coordinate system local to it in I_0, which we call the I_0 frame. For geometric convenience we assume that $|\psi(\mathbf{r},t_0)|$ has a cigarlike (i.e., ellipsoidal) shape, with longitudinal (L) and transverse (T) dimensions. (L here is not to be confused with the film thickness L in region II.) We take the longitudinal axis to lie along the direction of propagation toward region II. We choose a Z-X coordinate frame relative to the initial wave packet with the Z axis along the wave-packet longitudinal axis—i.e., along the direction of incidence—and with the Z axis making an

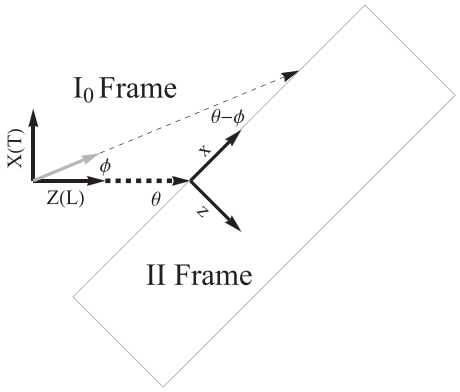

FIG. 1. Coordinate reference frames. The longitudinal axis of the wave packet in the I_0 frame has grazing angle of incidence θ on the film in the II frame, while a "virtual" ray along $\angle\phi$ in the I_0 frame is incident on the film at $\angle(\theta-\phi)$.

angle θ, the glancing angle incidence, with the x axis. These two systems are depicted in Fig. 1. The orientations of the two frames are thus related by

$$\begin{pmatrix} z \\ x \end{pmatrix} = \begin{pmatrix} \sin\theta & -\cos\theta \\ \cos\theta & \sin\theta \end{pmatrix} \begin{pmatrix} Z \\ X \end{pmatrix}. \tag{31}$$

For further simplicity we assume that in the I_0 frame, $A_{\mathbf{k}}$ factorizes as

$$A_{\mathbf{k}} = A(k_Z,k_X) = A_{\rm L}(k_Z)A_{\rm T}(k_X), \tag{32}$$

and model these as

$$A_{\rm L}(k_Z) = G(k_Z|k_{Z0},\Delta k_Z)e^{-i(k_Z-k_{Z0})Z_0} \tag{33a}$$

and

$$A_{\rm T}(k_X) = G(k_X|0,\Delta k_X), \tag{33b}$$

with G the normalized Gaussian,

$$G(k|k_0,\Delta k) = \frac{1}{\sqrt{2\pi}\,\Delta k} e^{-\frac{(k-k_0)^2}{2\Delta k^2}}. \tag{33c}$$

These definitions describe the initial wave packet (in the I_0 frame) as

$$\psi_{k_Z,k_X}(Z,X) = W(Z,X)e^{ik_{Z0}Z}, \tag{34a}$$

i.e., as the plane wave $e^{ik_{Z0}Z}$ "modified" by a Gaussian LT profile $W(Z,X)$,

$$W(Z,X) = e^{-\frac{1}{2}(Z-Z_0)^2\Delta k_Z^2} e^{-\frac{1}{2}X^2\Delta k_X^2}. \tag{34b}$$

The choice of Gaussian profiles is no surprise, of course, in dealing analytically with wave packets, although, strictly speaking, such shapes are not compactly supported. We do not believe, however, that this is a critical concern here.

While it is appropriate to specify a wave packet in terms of its Fourier content, as we have done in (33), the longitudinal (Z) and transverse (X) spatial dimensions of the wave packet are not then precisely defined. The matter is compounded by commonly loose references to wave-packet "sizes" or to "correlation" or "coherence" lengths, which may refer to different lengths in different contexts. It seems reasonable enough, however, to define *minimal* and *maximal* lengths $1/\Delta k_\ell$ and $6/\Delta k_\ell$, respectively, for $\ell = Z,X$. We delay further consideration of the "sizing" question until later.

Now in (30), for $D = 2$, the integration over $\omega_{\mathbf{k}}$ is most conveniently expressed in the I_0 frame as an integration of the polar angle ϕ, defined relative to the Z axis, as in Fig. 1. Then, using (31), the relationship between $\mathbf{k} = (k_z,k_z)$ and $\mathbf{k} = (k_Z,k_X) = (k\cos\phi, k\sin\phi)$ is simply

$$\begin{pmatrix} k_z \\ k_x \end{pmatrix} = \begin{pmatrix} \sin\theta & -\cos\theta \\ \cos\theta & \sin\theta \end{pmatrix} \begin{pmatrix} k\cos\phi \\ k\sin\phi \end{pmatrix} = k\begin{pmatrix} \sin(\theta-\phi) \\ \cos(\theta-\phi) \end{pmatrix}. \tag{35}$$

That is, a ray directed along *given* ϕ in the I_0 frame, has grazing angle of incidence $\theta-\phi$ on the film, as depicted in Fig. 1. For example, $\phi = 0$ corresponds to the L axis of the incident wave packet, and k_z and k_x thus are defined as usual for a plane wave incident at $\angle\theta$, while $\phi = \theta$ corresponds to perfect grazing incidence. Also in (30), let us again write $\mathbf{k} = k\hat{\mathbf{k}}$ and promote $\hat{\mathbf{k}}$ to argument status by taking $A_{\mathbf{k}} \to A_k(\hat{\mathbf{k}})$ and $\psi^s_{\mathbf{k}}(\mathbf{r}) \to \psi^s_k(\mathbf{r}|\hat{\mathbf{k}})$. Then the gated wave packet (30) becomes

$$\tilde{\psi}^s_k(\mathbf{r}) = \frac{2\pi m}{\hbar}\int_{\phi_1}^{\phi_2} A_k(\cos\phi,\sin\phi) \times \psi^s_k(z,x|\sin(\theta-\phi),\cos(\theta-\phi))\,d\phi, \tag{36}$$

where the limits of integration, $\phi_{1,2}$, will be set shortly. This represents a coherent average of $\psi^s_k(\mathbf{r}|\hat{\mathbf{k}})$ over a set of *virtual* plane-wave angles of incidence, weighted by the reciprocal space wave-packet amplitude $A_k(\hat{\mathbf{k}})$ along the k circle in the I_0 frame (see Fig. 2). The *coherent* superposition described here of virtual plane-wave incident angles "within" the wave packet of a *single* particle must be carefully distinguished—and separated—from an *incoherent* superposition of incident angles in a beam of distinguishable wave packets. This point and its experimental consequences are discussed in Part I.

Since $\psi^s_{\mathbf{k}}(\mathbf{r})$ is a *physical* scattering solution for the given setup (with detectors in region Ω_d), virtual glancing angles of incidence on the film—as defined by the angle of the wave

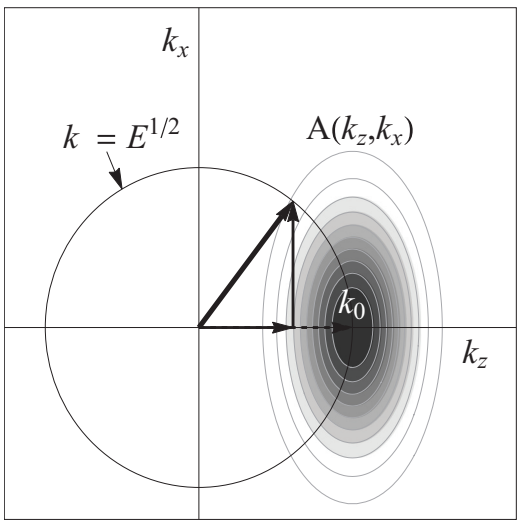

FIG. 2. Representation of I_0 and the Z-X frame.

packet's L axis to the film—are limited to the range $0 \leqslant \theta \leqslant \pi/2$. However, we must also allow for $\pi/2 \leqslant \theta - \phi \leqslant \pi$, because the reciprocal-space representation of the initial wave packet generally will have weight in directions $\hat{\mathbf{k}}$ that correspond to incidence at angles in this range. Thus, the allowed range of ϕ in (36) is restricted to $\theta - \pi \leqslant \phi \leqslant \theta$, and (36) thus becomes

$$\tilde{\psi}_k^s(\mathbf{r}) = \frac{2\pi m}{\hbar} \int_{\theta-\pi}^{\theta} A_k(\cos\phi, \sin\phi) \times \psi_k^s(z,x|\sin(\theta-\phi), \cos(\theta-\phi))\, d\phi. \quad (37)$$

In practice, the effective ϕ range of integration in (37) will be reduced by the shape of $A_k(\hat{\mathbf{k}})$ (again, see Fig. 2). For example, for $\psi(\mathbf{r},t_0) \approx e^{i\mathbf{k}_0\cdot\mathbf{r}}$, and with $k = |\mathbf{k}_0|$, the effective ϕ range will be confined to a small neighborhood of $\phi = 0$.

A. Specular-only reflection

Staying with $D = 2$, it is useful to apply (36) to the case of a perfectly smooth film, such that in (1), $U(\mathbf{r}) = U(z\hat{\mathbf{z}})$. Reflection, then, is purely specular; and for an incident plane wave $\psi^i(\mathbf{r}|\mathbf{k}) = e^{ik_z z}e^{ik_x x}$, the reflected wave ($s \to r$) is

$$\psi^r(\mathbf{r}|\mathbf{k}) = r(k_z)e^{-ik_z z}e^{ik_x x}, \quad (38)$$

where $r(k_z)$ is the reflection coefficient. (The dynamical theory of plane-wave specular reflection is summarized in [8], for example.) Thus, from (37), an incident wave packet produces the reflected wave

$$\tilde{\psi}_k^r(\mathbf{r}) = \frac{2\pi m}{\hbar} \int_{\theta-\pi}^{\theta} A_k(\cos\phi, \sin\phi)\, r[k\sin(\theta-\phi)] \times e^{-ik\sin(\theta-\phi)z}e^{ik\cos(\theta-\phi)x}\, d\phi. \quad (39)$$

It is important to notice in (39) that the z- and x-dependent plane-wave functions are averaged with respect to ϕ along with the reflection amplitude $r[k\sin(\theta-\phi)]$. Since the scattered wave is detected far from film surface, these sinusoidal factors will oscillate very rapidly with ϕ, causing the right-hand side to become very small in general. However, for specular reflection, we expect the detected signal to be observable only very near (z,x) lying along the specular ray, i.e., at $(z,x) = \mathcal{D}(-\sin\theta, \cos\theta)$, where $\mathcal{D}$ is the distance of the detector to the center of the film. Therefore, on *this* line,

$$e^{-ik\sin(\theta-\phi)z}e^{ik\cos(\theta-\phi)x} = e^{ik\mathcal{D}\cos(2\theta-\phi)}$$

in (39), where $\angle 2\theta$ is, in fact, the specular scattering angle. For a long cigar-shaped wave packet we can assume that $A_k(\hat{\mathbf{k}})$ is pancaked shaped, centered at $\mathbf{k}_0 = (k_{0Z},0)$ and with $\Delta k_X \ll \Delta k_Z$. Thus, for $\mathbf{k} \approx \mathbf{k}_0$, the effective range, $\pm\Delta\phi$, of ϕ about $\phi = 0$ is $\Delta\phi \approx \arctan \Delta k_X/k_{0Z}$, so that

$$\Delta\phi \approx \lambda_0/\Delta X \ll \pi/2,$$

using $\lambda_0 = 2\pi/k_0$ and $\Delta X = 2\pi/\Delta k_X$. We also assume here that the (real space) transverse width of the wave packet is large compared to the neutron wavelength, which likely will hold in most cases of interest, with the possible exception of ultracold neutrons. Thus, we can assume for this case that the effective limits of the ϕ integration in (39) are $0 \pm \Delta\phi$, with $\Delta\phi \ll 2\theta$, except for near-perfect grazing incidence. Then (39) becomes

$$\tilde{\psi}_k^r(\mathbf{r}) \approx \frac{2\pi m}{\hbar} e^{ik\mathcal{D}\cos(2\theta)} \times \int_{-\Delta\phi}^{\Delta\phi} A_k(\cos\phi, \sin\phi)\, r[k\sin(\theta-\phi)]\, d\phi. \quad (40a)$$

For all practical purposes under these conditions, we can also take $\theta - \phi \to \theta$ in this integral, leading to

$$\tilde{\psi}_k^r(\mathbf{r}) \approx r(k_z)e^{ik\mathcal{D}\cos(2\theta)} \frac{2\pi m}{\hbar} \int_{-\Delta\phi}^{\Delta\phi} A_k(\cos\phi, \sin\phi)\, d\phi = r(k_z)e^{ik\mathcal{D}\cos(2\theta)}c_k, \quad (40b)$$

in short, up to a normalizing constant c_k, the specular result for an incident plane wave.

The above line of analysis, while correct in its geometric detail, is tedious. The better way to the desired result is to formulate an ansatz for the measurable quantity of interest. In (54b), near the end of the next section, we define the measurable reflection amplitudes for a gated wave packet in the manner of a projective measurement, namely, as

$$\tilde{r}_{\mathbf{k}}(k_x^r) = \frac{\langle k_x^r|\tilde{\psi}_{\mathbf{k}}^r\rangle}{\langle k_x^i|\tilde{\psi}_{\mathbf{k}}^i\rangle}, \quad (41)$$

computed at $z = 0$ and specialized here to the case of $D = 2$. In other words, a gated reflection amplitude is the ratio of projections of the gated reflected and gated incident waves onto the plane waves implicit in the gated measurement. Since it is the specular reflection we wish to observe (the only allowed reflection in this example), we take $k_x^r = k_x^i = k\cos\theta$, and thus, from (39),

$$\begin{aligned}\langle k_x^r|\tilde{\psi}_{\mathbf{k}}^r\rangle &= \frac{2\pi m}{\hbar} \int_{\theta-\pi}^{\theta} A_k(\cos\phi, \sin\phi)\, r[k\sin(\theta-\phi)] \times \frac{1}{2\pi k}\delta(\cos(\theta-\phi) - \cos\theta)\, d\phi \\ &= \frac{2\pi m}{\hbar} \int_{\theta-\pi}^{\theta} A_k(\cos\phi, \sin\phi)\, r[k\sin(\theta-\phi)] \times \delta(\phi)\, \frac{d\phi}{2\pi k|\sin\theta|} \\ &= \frac{m}{\hbar k|\sin\theta|} A_k(1,0)\, r[k\sin(\theta)]. \end{aligned} \quad (42a)$$

where we have isolated $\phi = 0$ as the only acceptable solution of $\cos(\theta-\phi) = \cos\theta$, required to satisfy the Dirac δ function for given θ; the factor $|\sin\theta|^{-1}$ appearing in the second equality is the Jacobian of the requisite transformation, $\cos(\theta-\phi) \to \phi$. Similarly,

$$\langle k_x^i|\tilde{\psi}_{\mathbf{k}}^i\rangle = \frac{m}{\hbar k|\sin\theta|} A_k(1,0), \quad (42b)$$

obtained from (42b) by setting $r[k\sin(\theta-\phi)] = 1$; in effect, the incident beam is equivalent to a perfectly reflected specular beam.

Thus, at once from (41),

$$\tilde{r}_{\mathbf{k}}(k_x^r) = r[k\sin(\theta)] = r(k_z), \quad (43)$$

exactly as for an incident perfect plane wave. In other words, the shape of an incident wave packet is invisible for reflection from a perfectly smooth film along the *specular ridge*, i.e., for reflection angles satisfying the specular condition. We point out that this result also follows, with a small bit of reinterpretation, from (21), the case for gating when $D = 1$. The problem of plane-wave reflection from a perfectly smooth film can be mathematically reduced to one dimension.

For $U(\mathbf{r}) = U(z)$, the solution of the TISE in three dimensions,

$$-\frac{\hbar^2}{2m}\nabla^2\psi(\mathbf{r}) + U(z)\psi(\mathbf{r}) = \frac{\hbar^2}{2m}k^2\psi(\mathbf{r}),$$

has the form $\psi(\mathbf{r}) = \psi(z)e^{ik_x x}e^{ik_y y}$, where $\psi(z)$ thus satisfies

$$-\frac{\hbar^2}{2m}\partial_z^2\psi(z) + U(z)\psi(z) = \frac{\hbar^2}{2m}k_z^2\psi(z).$$

With $k^i = k, k^r = -k$, $|\psi^r\rangle = |k\rangle$, and $|\psi^r\rangle = r(k_z)|-k\rangle$, the combination of (21) and (41) directly gives $\tilde{r}(k^r) = r(k_z)$, since A_k again cancels out. As we will soon see, it is the simultaneous existence of specular and nonspecular reflections which bring the shape of the wave packet into play along the specular ridge through the phenomenon of *aliasing*, i.e., the appearance, in the simplest cases, of nonspecular reflection at the nominal specular angle.

On the other hand, returning to the two-dimensional case, let us take $k_x^r = k_x(\theta,\chi) = k\cos(\theta - \Delta)$ in (42); i.e., let us "look" slightly off the specular ridge, corresponding to a "rocking curve" with rocking angle Δ. (We define rocking curves in a more general context in Sec. IV 1.) Then,

$$\tilde{r}_{\mathbf{k}}[k_x(\chi)] = \frac{|\sin\theta|A_k[\cos\chi, \sin\chi]}{|\sin(\theta-\chi)|}\, r[k\sin(\theta-\chi)]. \quad (44)$$

Thus, in the "critical" region, near $\theta = 0$, where $|r[k\sin(\theta - \chi)] \approx 1|$, and assuming χ is small, the rocking curve provides a more-or-less direct measure of the transverse "shape" of the incident wave packet, via $A_k(1,\chi)$.

B. Nonspecular reflection

For the general case of nonspecular reflection (with $D = 3$), the reflected wave (in region $\mathrm{I_r}$) can be represented as

$$\psi_{\mathbf{k}}^r(\mathbf{r}) = \int a_{\mathbf{k}}^r(\mathbf{k}_\parallel^r)e^{i\mathbf{k}^r(\mathbf{k}_\parallel^r)\cdot\mathbf{r}}\,\frac{d^2k_\parallel^r}{(2\pi)^2}, \quad (45)$$

with the identification

$$\mathbf{k}^r(\mathbf{k}_\parallel^r) = \mathbf{k}_\parallel^r - k_z(k_\parallel)\,\hat{\mathbf{z}}, \quad (46)$$

where $k_z(k_\parallel) = \sqrt{k^2 - k_\parallel^2}$ for any $k_\parallel$. The scattering *coefficient* $a_{\mathbf{k}}^r(\mathbf{k}_\parallel^r)$ in (45) is defined in terms of the exact wave function in region II by

$$a_{\mathbf{k}}^r(\mathbf{k}_\parallel^r) = \frac{1}{2ik_z(k_\parallel^r)}\int_{\mathrm{II}} e^{-i\mathbf{k}^r(\mathbf{k}_\parallel^r)\cdot\mathbf{r}}q(\mathbf{r})\psi_{\mathbf{k}}(\mathbf{r})\,d^3r, \quad (47)$$

where $q(\mathbf{r}) = 4\pi\rho(\mathbf{r})$, and where $\rho(\mathbf{r}) = 2mU(\mathbf{r})/(4\pi\hbar^2)$ is the scattering length density. (We assume, for now, a free film.) Also in (47),

$$\psi_{\mathbf{k}}(\mathbf{r}) = e^{i\mathbf{k}\cdot\mathbf{r}} + \psi_{\mathbf{k}}^s(\mathbf{r}), \quad (48)$$

where $\psi_{\mathbf{k}}^s(\mathbf{r})$ is the scattered component of the total wave function defined by the physical solution to the TISE. The solution form in (48) applies everywhere, but in region $\mathrm{I_r}$ we will refer to its scattered component as the reflected part; i.e., $\psi_{\mathbf{k}}^s(\mathbf{r}) = \psi_{\mathbf{k}}^r(\mathbf{r})$ for $\mathbf{r} \in \mathrm{I_r}$. Now at $z = 0$, the boundary between I and II, (45) gives

$$\lim_{z\to 0^+}\psi_{\mathbf{k}}^r(\mathbf{r}) = \psi_{\mathbf{k}}^s(\mathbf{r}_\parallel) = \int a_{\mathbf{k}}^r(\mathbf{k}_\parallel^r)e^{i\mathbf{k}_\parallel^r\cdot\mathbf{r}_\parallel}\,\frac{d^2k_\parallel^r}{(2\pi)^2}, \quad (49)$$

expressing the scattered wave on the nominal surface of the film as a two-dimensional Fourier transform of the reflection coefficient with respect to all possible reflected rays projected onto the surface. Thus, the reflection coefficient itself is the corresponding inverse Fourier transform of the reflected wave on the $z = 0$ plane, viz.,

$$a_{\mathbf{k}}^r(\mathbf{k}_\parallel^r) = \int_{\mathrm{II}} e^{-i\mathbf{k}_\parallel^r\cdot\mathbf{r}_\parallel}\psi_{\mathbf{k}}^r(\mathbf{r}_\parallel)\,d^2r_\parallel. \quad (50)$$

The reflected wave thus can be said to "carry away" its $z = 0$ imprint into region $\mathrm{I_r}$ by adding to each $\mathbf{k}_\parallel^r$ the appropriate $k_z(k_\parallel^r)$. For the $D = 2$ (z-x) problem the relevant planar Fourier transform is a one-dimensional transform along the x axis, and (50) becomes

$$a_{\mathbf{k}}^r(k_x^r) = \int_{-\infty}^{\infty} e^{-ik_x^r x}\psi_{\mathbf{k}}^r(x,0)\,dx, \quad (51)$$

where $a_{\mathbf{k}}^r(k_x^r)$ means $a_{\mathbf{k}}^r(k_x^r\hat{\mathbf{x}})$, etc. The integral in (51) can be interpreted as the (un-normalized) projection of $\psi_{\mathbf{k}}^r(x,0)$ onto the "observed" plane-wave state $e^{ik_x^r x}$; in Dirac notation, $a_{\mathbf{k}}^r(k_x^r) = \langle k_x^r|\psi_{\mathbf{k}}^r\rangle$ at $z = 0$. In order to extract the associated reflection *amplitudes*, let us define

$$a_{\mathbf{k}}^i(k_x) = \int_{-\infty}^{\infty} e^{-ik_x x}e^{ik_x x}\,dx = \lim_{\mathcal{L}\to\infty}\mathcal{L} \quad (52a)$$

for the *incident* beam, where $\mathcal{L}$ is the nominal macroscopic length of the (one-dimensional) film. Then

$$r_{\mathbf{k}}(k_x^r) = \frac{a_{\mathbf{k}}^r(k_x^r)}{a_{\mathbf{k}}^i(k_x)} = \lim_{\mathcal{L}\to\infty}\frac{a_{\mathbf{k}}^r(k_x^r)}{\mathcal{L}}, \quad (52b)$$

which is dimensionless.

In general, in D dimensions, $a_{\mathbf{k}}^r(k_x^r)$ has dimension Length^{D-1}, as seen in (50) for dimensionless $\psi_{\mathbf{k}}(\mathbf{r})$. Typically, especially for periodic structures, this dimensionality reveals itself in the dimensions of Dirac δ functions, as in, say, for $D = 2$, $a_{\mathbf{k}}^r(k_x^r) = 2\pi\, r_{\mathbf{k}}(k_x^r)\delta(k_x^r - k_{xm}^r)$, where $k_{xm}^r = k_x + G_{xm}$ and G_{xm} is a reciprocal lattice vector along x. Then, using the rule in (52), $r_{\mathbf{k}}(k_x^r) \to r_n(k_x^r)\delta_{nm}$, where δ_{nm} is the Kronecker δ, and $\delta(k_x^r - k_{xm}^r)/\mathcal{L} \to \delta_{nm}$. The case of a film in the form of a grating is discussed in detail in Sec. IV.

For $D = 3$, (52) becomes

$$a_{\mathbf{k}}^i(\mathbf{k}_\parallel) = \lim_{\mathcal{S}\to\infty}\mathcal{S},$$

where $\mathcal{S}$ is the nominal area of the film surface; and then the dimensionless reflection coefficient is

$$r_{\mathbf{k}}(\mathbf{k}_\parallel^r) = \frac{a_{\mathbf{k}}^r(\mathbf{k}_\parallel^r)}{a_{\mathbf{k}}^i(\mathbf{k}_\parallel)} = \lim_{\mathcal{S}\to\infty}\frac{a_{\mathbf{k}}^r(k_x\mathbf{k}_\parallel^r)}{\mathcal{S}}. \quad (53)$$

The general result in (30) is now

$$\tilde{\psi}^s_k(\mathbf{r}) = \frac{2\pi m k^{D-2}}{\hbar}\int \frac{d^2k^r_\parallel}{(2\pi)^{D-1}} \times \int A_{\mathbf{k}} a^r_{\mathbf{k}}(\mathbf{k}^r_\parallel) e^{i\mathbf{k}^r(\mathbf{k}^r_\parallel)\cdot\mathbf{r}} \frac{d^{D-1}\omega_{\mathbf{k}}}{(2\pi)^D}, \tag{54a}$$

and the *observable* reflection amplitude $\tilde{r}_{\mathbf{k}}(\mathbf{k}^r_\parallel)$, along the direction of $\mathbf{k}^r$, is defined by

$$\tilde{r}_{\mathbf{k}}(\mathbf{k}^r_\parallel) = \frac{\langle \mathbf{k}^r_\parallel | \tilde{\psi}^r_{\mathbf{k}}\rangle}{\langle \mathbf{k}^i_\parallel | \tilde{\psi}^i_{\mathbf{k}}\rangle}, \tag{54b}$$

where $\mathbf{k}^i_\parallel = \mathbf{k}_\parallel$; the gated incident wave $\tilde{\psi}^i_{\mathbf{k}}$ (at $z = 0$), needed in (54b), can be obtained from (54a) by replacing $a^r_{\mathbf{k}}(\mathbf{k}^r_\parallel)$ with $a^r_{\mathbf{k}}(\mathbf{k}^i_\parallel) = \delta(\mathbf{k}^r_\parallel - \mathbf{k}_\parallel)$. The application of (54b) to the special case of reflection from a perfectly smooth film was shown in the previous section, at Eqs. (42) and (43).

Needless to say, (54) hides details that can be difficult to treat in some circumstances. However, these are better worked out in the contexts of specific problems, and we now turn our attention to an important class of such applications.

IV. IMPLEMENTATION II: GATED REFLECTION FROM A GRATING

Here we apply the general case of Sec. IV to the case of reflection from a perfect grating. Not only does this specialization allow us to reveal more of the underlying mathematical structure of the scattering of gated wave packets, but it also bears directly on an important class of problems of interest, including, of course the measurements described in the companion work [2]. To this end we first work out some general consequences of gated wave-packet reflection from ruled gratings, assuming that the requisite plane-wave solutions for gratings are known. In fact, this is a very difficult problem in its own right in the *dynamical* scattering regime of primary interest to us. Therefore, in the Appendix we develop an exact solution method for the particular case of rectangular gratings, i.e., gratings whose rulings have rectangular-barrier-shaped scattering length density profiles. In order to avoid mathematical complications related to reflection from a film supported on a substrate, we imagine, for now, a two-component grating with the space between lines filled with material nearly transparent to neutrons, such as silicon, so that the grating film can be considered to be freely suspended. In the Appendix, we show how to include a substrate in the context of the solution method developed there for perfect plane-wave scattering from gratings.

From here on we consider only $D = 2$, which is sufficient for the purpose at hand. Let us take the plane of incidence (as would be defined by a ray of an incident plane wave) to be the z-x plane of region I with the grating lines running along the y axis; i.e., a ray incident in the z-x plane is perpendicular to the direction of the grating lines. In this geometry the scattering problem can be considered as two dimensional, since the film potential $U(\mathbf{r}) \to \rho(\mathbf{r}) = \rho(z,x)$ is smooth along the y axis. Then for a grating with rectangular lines (i.e., lines having vertical sides) of thickness (along z) L_g and period (along x) T_g,

$$q(z,x) = \sum_{n=-\infty}^{\infty} q_n(z) e^{iG_n x} = \overline{q}(z) + \sum_{n\neq 0} q_n(z) e^{iG_n x}, \tag{55a}$$

where the G_n are the reciprocal lattice vectors for the grating,

$$G_n = \frac{2\pi n}{T_g} = nk\tau, \tag{55b}$$

for integer n, and where $\tau = \lambda/T_g$ for specified $k = 2\pi/\lambda$. For a rectangular profile,

$$q_n(z) = \begin{cases} q_n(0), & 0 \leqslant z \leqslant L, \\ 0, & \text{otherwise.} \end{cases} \tag{55c}$$

In (55a), $\overline{q}(z) = q_0(z) = q_0(0)$ is the average value of the grating along the x axis, since the average of the summation over n, absent $n = 0$, is zero. Furthermore, assuming a real-valued $\rho(z)$, we require that $q^*_n(z) = q_{-n}(z)$; for a choice of the x origin about which $q(z,-x) = q(z,x)$, this becomes $q_{-n}(z) = q_n(z)$.

At any z in II, the scattered component of the wave function is a Bloch function along x,

$$\psi^s_{\mathbf{k}}(z,x) = e^{ik_x x} U^s_k(k_x,z,x), \tag{56a}$$

where $U^s_k(k_x,z,x + T_g) = U^s_k(k_x,z,x)$, so that

$$U^s_k(k_x,z,x) = \sum_{n=-\infty}^{\infty} U^s_{kn}(k_x,z) e^{iG_n x}. \tag{56b}$$

Note that because of (46), the k_z dependence of $U^s_{kn}(k_x,z)$ is implicit. Because the wave function is everywhere continuous, at $z = 0$ we can identify $\psi^s_{\mathbf{k}}(0,x)$ in II with $\psi^r_{\mathbf{k}}(0,x)$ from I. Then, by inserting (56) into (51), we easily get

$$\begin{aligned} a^r_{\mathbf{k}}(k^r_x) &= 2\pi \sum_n U^r_{kn}(k_x,0)\delta\left(k^r_x - k^r_{xn}\right) \\ &= 2\pi \sum_n r^r_{kn}(k_x)\delta\left(k^r_x - k^r_{xn}\right), \end{aligned} \tag{57}$$

where

$$k^r_{xn} = k_x + G_n, \tag{58}$$

and where the $r^r_{kn}(k_x)$, for $n = 0,\pm1,\pm2,\ldots$, are the reflection amplitudes for the grating. Therefore, from (45),

$$\begin{aligned} \psi^r_{\mathbf{k}}(\mathbf{r}) &= \sum_n U^r_{kn}(k_x,0) e^{-ik^r_z(k^r_{xn})z} e^{ik^r_{xn}x} \\ &= \sum_m r_{km}(k_x) e^{-ik_z(k^r_{xn})z} e^{ik^r_{xn}x} \end{aligned} \tag{59}$$

in region $\mathrm{I_r}$. The reflected wave in $\mathrm{I_r}$, therefore, is a superposition of all allowed reflected plane waves. In (59), $k^r_z(k^r_{xn}) = -\sqrt{k^2 - k^r_{xn}}$ is defined as a negative number, since the reflected wave travels away from the surface, while our surface normal is directed into the surface. When (59) is inserted into (37), the gated wave packet for the grating becomes

$$\tilde{\psi}^r_k(\mathbf{r}) = \sum_n \int_{\theta-\pi}^{\theta} d\phi\, A_k(\phi)\, r^r_{kn}(\theta - \phi) \times e^{ik_{zn}(\theta-\phi)z} e^{ik_{xn}(\theta-\phi)x}. \tag{60}$$

Our earlier notation, while precise, proves cumbersome for the ensuing development. So, in (60) and in the subsequent formulas, we simplify as follows:

$$k_z^r\big[k_{xn}^r(\theta)\big] \to k_{zn}^r(\theta), \quad r_{\mathbf{k}}\big[k_{xn}^r(\theta)\big] \to r_n(\theta),$$

and

$$A_k(\cos\phi, \sin\phi) \to A_k(\phi).$$

The constant-k constraint generally is left implicit, except in $A_k(\phi)$, and some arguments are dropped when not immediately essential. If now we consider a spherically shaped detector a distance $\mathcal{D}$ from a reference point on the sample, then with $z = -\mathcal{D}\sin\theta$ and $x = \mathcal{D}\cos\theta$, each term in the summation over n is to be "observed" at angle $\theta_n^r = -\arctan[k_{xn}^r(\theta)/k_{zn}^r(\theta)]$ [for real-valued $k_{zn}^r(\theta)$].

The projection rule (54) applied to (60) leads in a few steps [similar to those in Eq. (42)] to observable specular ($m = 0$) and nonspecular ($m \neq 0$) reflection amplitudes, at incident angle θ, represented by

$$\tilde{r}_m(\theta) = \sum_n \tilde{A}_k(\theta, n-m) r_n(\theta - \phi_{n-m}(\theta)). \tag{61a}$$

For further notational simplification we have defined

$$\tilde{A}_k(\theta, n-m) = \tilde{A}_k(\phi_{n-m}(\theta)), \tag{61b}$$

where

$$\tilde{A}_k(\phi) = \frac{|\sin\theta|}{|\sin(\theta-\phi)|}\frac{A_k(\phi)}{A_k(0)}, \tag{61c}$$

and $\tilde{A}_k(0) = 1$. In (61b) $\phi_{n-m}(\theta)$ is the physical solution of

$$\cos(\theta - \phi_{n-m}) + n\tau = \cos\theta + m\tau, \tag{62}$$

which we refer to as the *aliasing equation*, since it defines a virtual incident ray producing the same reflection angle as the wave-packet incident ray but corresponding to a different reciprocal lattice vector. The denominator of the transcendental ratio in (61c) is the Jacobian factor resulting from the reduction of the Dirac δ function associated with the solution of (62), normalized in the numerator by the Jacobian factor for the incident wave packet. We note that $\tilde{A}_k(0) = 1$, which applies to all instances of $n = m$. The physical solutions of (62) are the ones associated with real-valued $k_{zn}(\theta)$ and are single-valued functions of θ. The aliasing equation also has "unphysical" solutions corresponding to imaginary values of $k_{zn}(\theta)$, which must not be counted.

In other words, (61b) expresses the appearance at reflected wave vector $k_{xm}^r = k\cos\theta + G_m$ of a reflection expected at wave vector $k_{xn}^r = k\cos\theta + G_n$ but associated with a virtual wave vector incident at $\theta - \phi_{mn}$. Then, according to (61), the gated reflection amplitude $\tilde{r}_m(\theta)$ is a weighted sum over all possible aliased reflection amplitudes consistent with the nominal incident angle θ.

On the specular ridge, where $m = 0$, the aliasing equation reads as

$$\cos(\theta - \phi_n) + n\tau = \cos\theta, \tag{63}$$

so that we can write

$$\tilde{r}_m(\theta) = r_m(\theta) + \sum_{n\neq 0} \tilde{A}_k(\theta, n) r_n(\theta - \phi_n(\theta)), \tag{64}$$

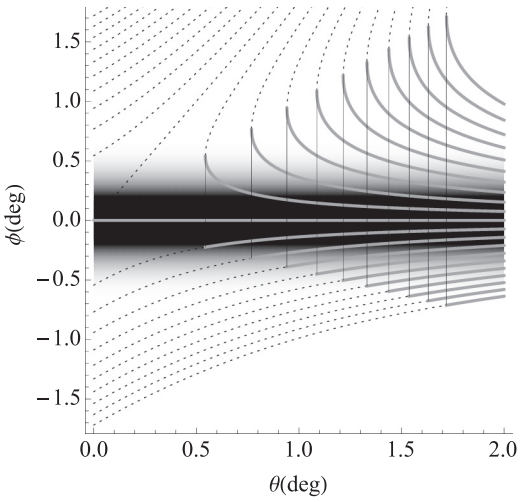

FIG. 3. $\phi_n(\theta)$ vs θ (angles in degrees), as determined by the solutions of (63). In solid gray, physical solutions of the aliasing equation along the specular ridge, ordered to the right for increasing $|n|$, with negative (positive) ϕ_n corresponding to positive (negative) n. The dotted vertical lines indicate the "horizon" incident angles θ_n^h, as defined by (65). The horizontal shading schematically indicates the θ-independent "weight" of $A_k(\phi)$, assuming a Gaussian profile; the ϕ_n get less weight the further they are from $\phi = 0$. The solutions shown here where computed for $\tau = 4.75 \times 10^{-5}$, corresponding to $T_g = 10\ \mu$m and $\lambda = 4.75$ Å.

exhibiting the wave-packet reflection amplitude $\tilde{r}_m(\theta)$ as the associated plane-wave reflection amplitude $r_m(\theta)$ plus the corrections caused by aliasing of all *other* reflection amplitudes. At a specified n there are physical solutions of (63) only for $\theta \geqslant \theta_n^h$, the "horizon" incident angle,

$$\theta_n^h = \cos^{-1}(1 - |n|\tau). \tag{65}$$

There are $2|n| + 1$ such solutions between adjacent horizons θ_n^h and θ_{n+1}^h for $n = 0, 1, \ldots$, and $\phi_0 = 0$ is a solution for all θ. These properties are summarized in Fig. 3 for the case $T_g = 10\ \mu$m and $\lambda = 4.75$ Å, corresponding to $\tau = 4.75 \times 10^{-5}$. As the figure illustrates, aliasing at small $|n|$ becomes insignificant as the transverse width of the wave packet becomes large, i.e., as the width of the function $A_k(\phi)$ becomes small (represented by the horizontal shading in the figure for Gaussian weighting).

Again for $\tau = 4.75 \times 10^{-5}$, Fig. 4 shows $\tilde{A}_k(\theta, n)$ for several n and for two values of the wave-packet transverse

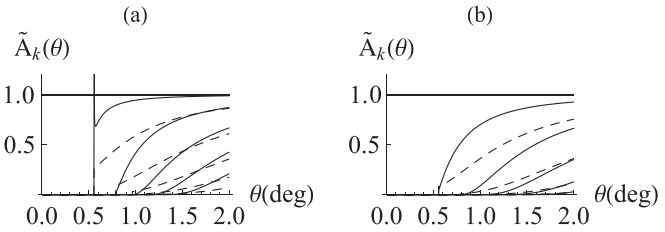

FIG. 4. $\tilde{A}_k(\theta) = \tilde{A}_k(\theta, n)$ vs θ (in degrees) for $n = 0$ to $n = \pm 5$ (from left to right), as determined by the solutions of (63), and for two choices of the wave-packet transverse dimension: (a) $\Delta_X = 0.1\ \mu$m; (b) $\Delta_X = 0.15\ \mu$m. Solid lines, $n \leqslant 0$; dotted lines, $n > 0$. The wave-packet longitudinal dimension is $\Delta_Z = 10\ \mu$m. Other parameters are as in Fig. 3.

dimension, $\Delta_X = 0.1\ \mu$m and $\Delta_X = 0.15\ \mu$m for fixed longitudinal dimension $\Delta_Z = 10\ \mu$m. The spike in (a) is caused by the divergence of the Jacobian factor in (61c) at the $n = -1$ horizon, significantly moderated by the exponential decrease of $A_k(\phi)$ with increasing ϕ. Indeed, horizon spikes for $n = -2, -3, \ldots$, are hardly visible on the scale of the figure. The difference between the plots in (a) and (b) also illustrates the sensitivity to Δ_X in this regime of parameters. It is also worth noting that larger values of Δ_Z have very little effect on these graphs for the indicated τ and range of n; for $\Delta_Z \gg \lambda$, the wave packet's longitudinal behavior effectively is that of a perfect plane wave.

It follows from (64) that when $\theta < \theta_1^h$, $\tilde{r}_0(\theta) = r_0(\theta)$, the result for an incident perfect plane wave, as if $A_k \equiv 0$. That is, in the critical—or dynamical—reflection region, where $\theta \to 0$, the specular ridge tends to be insensitive to wave-packet dimensions—for those dimensions commensurate with and greater than the grating period.

1. *Gated wave packets and rocking curves*

When observing sharp reflection peaks in practice, it can be difficult to precisely "hit" a desired reflection angle. The well-known idea of a rocking curve is to get close and then scan along a "curve" of angles guaranteed to intersect the desired peak or ridge [9]. For our grating, say that the reflection of interest occurs at an angle corresponding to $k^r_{mx}/k = \cos\theta + m\tau$. This location also can be described by an offset angle of incidence, $\theta \to \theta - \chi_m^{(0)}$, such that

$$k^r_{mx}/k = \cos(\theta - \chi_m^{(0)}), \tag{66a}$$

where

$$\chi_m^{(0)} = \theta - \cos^{-1}(\cos\theta + m\tau), \tag{66b}$$

with $\chi_0^{(0)} = 0$; this, of course, is simply the geometry of the Ewald sphere used to identify possible nonspecular scattering events in crystals, here applied to the reciprocal space of the grating. A continuous scan that intersects this reflection can be defined by taking $\chi_m^{(0)} \to \chi_m(\Delta) = \chi_m^{(0)} - \Delta$ for continuous Δ, i.e.,

$$k^r_{mx}/k \to \cos(\theta - \chi_m) = \cos\left(\theta - \chi_m^{(0)} - \Delta\right). \tag{66c}$$

In effect, we can view this scan as taking m, the integer index of the reflection, into a real variable $\mu(\Delta)$. Indeed, to first order in Δ in (66),

$$\mu(\Delta) \approx m - \frac{\Delta}{\tau} k^r_{zm}(\theta)/k = \left(1 - \frac{k^r_{zm}}{G_m}\Delta\right)m.$$

This is mathematically equivalent to a local Δ-dependent distortion of the reciprocal lattice itself (equivalently, the grating Ewald sphere), taking $G_m \to G_m(\Delta)$ with

$$G_m(\Delta) \equiv G_m - k^r_{zm}\Delta + O(\Delta^2).$$

On the reflectometer, assuming a nonzero linewidth, we may treat the observation angle of the reflection as a function of Δ, i.e., take $\theta^{\rm obs} \to \theta^{\rm obs}(\Delta) = \theta - \chi(\Delta)$, or, for fixed $\theta^{\rm obs}$, treat the incident angle as a function of Δ, i.e., take $\theta \to \theta(\Delta) = \theta^{\rm obs} + \chi(\Delta)$. In fact, depending on instrumentation, both $\theta^{\rm obs}$ and θ may need to be varied such that $\theta(\Delta) - \theta^{\rm obs}(\Delta) = \chi(\Delta)$ for fixed Δ. For the purposes of the mathematical exposition, we prefer to treat θ as fixed along the rocking curve.

The aliasing equation along this rocking curve is

$$\begin{aligned}\cos(\theta - \phi_{n,m}) + n\tau &= \cos\left(\theta - \chi_m^{(0)} - \Delta\right)\\ &= \cos[\cos^{-1}(\cos\theta + m\tau) - \Delta],\end{aligned} \tag{67a}$$

using (66b). For $\Delta = 0$ this becomes

$$\cos(\theta - \phi_{n,m}) + n\tau = \cos\theta + m\tau, \tag{67b}$$

which is just (62) for $\phi_{n,m} = \phi_{n-m}$. The formal solution of (67a), with $\phi_{n,m} \to \phi_{n,m}(\Delta|\theta)$, is

$$\begin{aligned}\phi_{n,m}(\Delta|\theta) &= \theta - \cos^{-1}\left[\cos\left(\theta - \chi_m^{(0)} - \Delta\right) - n\tau\right]\\ &= \theta - \cos^{-1}\{\cos[\cos^{-1}(\cos\theta + m\tau) - \Delta] - n\tau\}.\end{aligned} \tag{67c}$$

By $\cos^{-1}$ here we mean the inverse satisfying $\cos^{-1}\cos\theta = \theta \mod 2\pi$ for any θ. This corresponds to the arccos function, as defined in Abramowitz and Stegun [10] and is to be distinguished from the principal value function, Arccos, for which $\mathrm{Arccos}\cos\theta = |\theta|$ for real θ. The Arccos function normally is the one encountered in computational environments. Now near $\Delta = 0$, (67c) becomes

$$\phi_{n,m}(\Delta|\theta) = \phi_{n-m}(\theta) + \frac{k^r_{zm}(\theta)}{k^r_{z(n-m)}(\theta)}\Delta + O(\Delta^2), \tag{68a}$$

where θ is assumed to be above the m and $n - m$ horizons. In particular, for $n = m$,

$$\phi_m(\Delta|\theta) \equiv \phi_{m,m}(\Delta|\theta) = \frac{k^r_{zm}(\theta)}{k^r_{z0}(\theta)}\Delta + O(\Delta^2), \tag{68b}$$

since $\phi_0 = 0$. [It is important to note the distinction between $\phi_{m,n}(\theta)$ and the rocking curve trajectory $\phi_{m,n}(\Delta|\theta)$]. Therefore, for $m = 0$, i.e., along the rocking curve "transverse" to the specular ridge (see below), $\phi_{0,0}(\Delta|\theta) \approx \Delta$.

The reflection amplitudes on the rocking curve are $\tilde{r}_m(\theta) \to \tilde{r}_m(\Delta|\theta)$, where

$$\begin{aligned}\tilde{r}_m(\Delta|\theta) = {}& \tilde{A}_k(\phi_m(\Delta|\theta))r_m(\theta - \phi_m(\Delta|\theta))\\ &+ \sum_{n\neq m}\tilde{A}_k(\phi_{n-m}(\Delta|\theta))r_n(\theta - \phi_{n-m}(\Delta|\theta)).\end{aligned} \tag{69}$$

For wave packets having sufficiently large Δ_X, so that aliasing can be ignored, the first term on the right-hand side of (67c) gives the "natural" (i.e., coherent) line shape of the mth reflection as the function $\tilde{A}_k(\phi_m(\Delta|\theta))$. Assuming for simplicity a Gaussian shape for $\tilde{A}(\phi_m(\Delta|\theta)) \to \tilde{A}_m(\Delta|\theta)$ near $\Delta = 0$, i.e.,

$$\tilde{A}_m(\Delta|\theta) \approx e^{-\frac{\Delta^2}{2\sigma_m^2}},$$

we get from (68b) that the angular dispersion near the center of line m along the rocking curve is

$$\sigma_m \approx \frac{1}{k\sigma_X}\left|\frac{k^i_z(\theta)}{k^r_{zm}(\theta)}\right|. \tag{70}$$

Thus, $\sigma_0 \approx 1/k\sigma_X$ determines the natural width of the specular ridge, and $\sigma_{-|m|} < \sigma_0 < \sigma_{|m|}$ for $m \neq 0$. Figure 5 shows examples of $\tilde{A}(\Delta|\theta)$ for two values of Δ_X. For the smaller

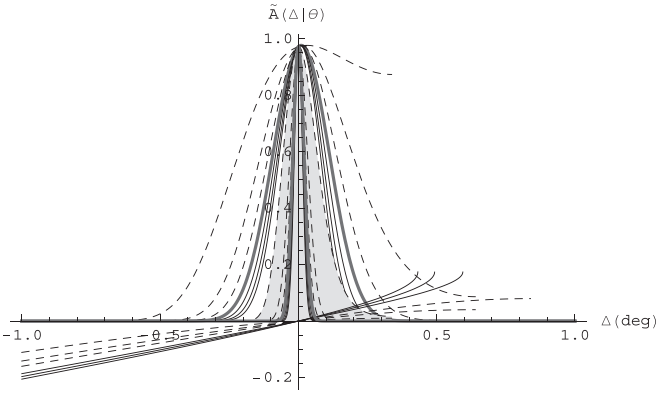

FIG. 5. "Line shapes" $\tilde{A}(\Delta|\theta)$ vs Δ (in degrees) along rocking curves [in θ for fixed θ; see (69)] for $m = 0$ (thick gray line), $m = -3,-2,-1$ (solid line), and $m = 1,2,3$ (dashed line); for $\Delta_X = 0.1\ \mu$m and $\Delta_X = 0.5\ \mu$m (shaded). The wave-packet longitudinal dimension is $\Delta_Z = 10\ \mu$m. Other parameters are shown on the figure or are as in Fig. 3. The $\phi_{m,m}(\Delta|\theta)$ trajectories (which are independent of wave-packet shape) are also shown on an arbitrary scale. Horizon effects are clearly seen for $\Delta > 0$.

value, the plots exhibit noticeable asymmetry associated with horizon effects as $\Delta \to \theta$; these are effectively suppressed, i.e., rendered unobservable, by the exponential decay of the line shape. Notice that Δ is defined relative to the line position, as defined in (66), so that each of the profiles in Fig. 5 lies on a different rocking curve.

Figure 6 compares the $m = +1$ line measured in Part I with the corresponding predicted rocking curve. The points correspond to the raw data, shifted from the actual peak position at 0.5°. The thin solid line is a model-independent fit of the raw data; angular resolution was tight, and therefore the result of the deconvolution of the incoherent instrumental beam resolution is nearly indistinguishable from this curve. The predicted line shape is essentially a Gaussian here. The resulting transverse correlation length is approximately 1.13 μm full width at half maximum (FWHM). Refer to Part I, Sec. VI and Tables III and IV. Similar agreement is obtained for the measured $m = -1$ line, as discussed in Part I.

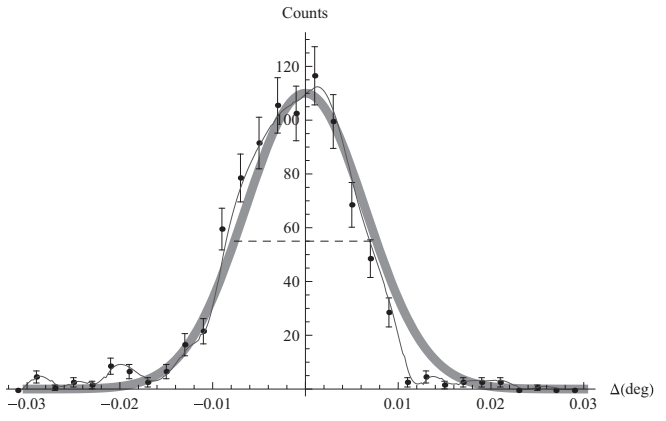

FIG. 6. Comparison of the measured $m = +1$ off-specular line from Part I for the $T_g = 20\ \mu$m ("10 + 10") grating with the prediction (heavy gray line). The dashed horizontal line is the predicted FWHM (see text).

The rocking curve specified here, when expressed in terms of wave-vector transfers, is also known as a *transverse scan*. Let $\theta_m^{\rm obs}$ be the angle at which the reflection indexed by m is observed. The wave-vector transfers for this reflection, Q_{mx} and Q_{mz}, are

$$Q_{mx}/k = \cos\theta_m^{\rm obs} - \cos\theta = \cos(\theta - \chi_m) - \cos\theta$$

and

$$Q_{mz}/k = -\sin\theta_m^{\rm obs} - \sin\theta = -[\sin(\theta - \chi_m) - \sin\theta],$$

where for Q_{mz} we have reversed the sign of $\theta_m^{\rm obs}$ to be consistent with our definition of the z axis. After a bit of trigonometry one finds that

$$Q = \sqrt{Q_{mx}^2 + Q_{mx}^2} = 2k\sin\left(\theta - \frac{\chi_m}{2}\right),$$

and then

$$Q_{mx}/k = Q\sin\left(\frac{\chi_m}{2}\right),$$

and

$$Q_{mz}/k = Q\cos\left(\frac{\chi_m}{2}\right).$$

Take note of the interchange of the sine and cosine here. Indeed, since over the range of θ typically of interest, χ_m is small, it follows that $Q_{mz} \approx 2k\sin\theta$ along the rocking curve. Observed changes on the rocking curve thus are mostly associated with wave-vector transfers along the x axis, the axis "transverse" to z.

V. CONCLUSIONS

The material above presents a comprehensive theoretical approach to the problem of elastic scattering of prepared wave packets as observed by standard neutron spectroscopy. The central results are summarized by the general representation of the scattered gated wave packet and the associated scattering (here reflection) amplitudes found in Eq. (54) and explicit expressions for the specular and nonspecular reflection amplitudes in Eqs. (64) and (69), respectively. These represent special cases of the general result in Eq. (61). In summary, the observable neutron reflectivities for prepared wave packets are completely determined by coherent, weighted summations of the exact dynamical reflection amplitudes for the plane-wave problem, the weighting depending only on the geometrical properties of the isolated wave packet with the energy gating defining exactly how these properties are sampled by an angular scan.

The main idea of this approach, as discussed in Sec. II, has been to resolve the dichotomy that while wave packets are nonstationary solutions of the time-dependent Schrödinger equation, elastic scattering theory, almost universally, assumes stationary states, i.e., solutions of the time-independent Schrödinger equation. Our resolution has been to obtain a stationary-state solution of the scattering that incorporates the main effects of time-dependent scattering by using the notion of energy-gated wave packets, namely the distorted wave packet that corresponds to the fixed incident energy ascribed to the incident beam in the analysis of the scattering.

The general picture of the scattering that results from gating is conceptually straightforward; the incident wave packet defines a totally *coherent*—i.e., pure state—collection of exact (i.e., dynamical) plane-wave solutions of the "same" scattering problem. With a proper definition of the observable scattering amplitudes as ratios of projections of the gated wave-packet scattering, shown in Eq. (54b), the resulting amplitudes are just weighted sums of plane-wave scattering amplitudes, the weighting depending on the Fourier content of the incident wave packet on the energy shell and incorporating the coherent *aliasing* due to misidentification of incident angles associated with measured scattering angles. In casual terms, the single-particle gated wave packet is a *coherent* analog of the *incoherent* angular dispersion determined by instrumental settings independent of the incident wave packets in the beam.

We have treated the particulars of the gating idea in the context of reflectometry for several reasons. First, the theory was motivated by the measurements of neutron reflection from ruled gratings described in detail in Part I of this study [2]. Second, the idealized "slab" reflection geometry allows for an easy spatial separation of the several distinct regions associated with different parts of the total wave function, as was described in Sec. III. These ideas certainly can be applied to other scattering conditions as well, including, say, small-angle scattering, where the scattered beam of interest there is analogous to the reflected wave here, while the forward scattered beam there is the analog of the transmitted beam here. We have developed implementation details for the grating problem not only for the first reason above but also because of the conceptually and mathematically convenient separability (i.e., the discrete nature) of the reciprocal space attached to gratings. Detailed generalizations to nonperiodic scatterers should not be too difficult, albeit not trivial, depending on the difficulty of the concomitant plane-wave problem. Third, and most important, the study of large-period gratings in Part I shows that for neutron beams the localization of the incident wave packet is observable in reflectometry and amenable to quantitative analysis with gated wave-packet theory once instrumental and sample effects outside the theory have been carefully removed from the data.

For the specific application of the gated wave-packet theory to ruled gratings it remains to obtain the required dynamical solutions of the attendant plane-wave scattering problem. We deal with this problem in some detail in the Appendix for the two-dimensional grating problem that was defined in Sec. III. An alternative treatment is described by Ashkar *et al*. [6].

ACKNOWLEDGMENT

The author has benefited greatly from extended discussions of this problem with C. F. Majkrzak.

APPENDIX: PLANE-WAVE REFLECTION FROM A RULED GRATING

In order to compute the formula for the gated reflection amplitudes in (60) we need the plane-wave reflection coefficients $r_{kn} = U^r_{kn} = U^s_{kn}(z=0)$ for the grating. We obtain these from the physical solutions of the Schrödinger equation in region II,

$$-\nabla^2_{z,x}\psi_{\mathbf{k}}(z,x) + q(z,x)\psi_{\mathbf{k}}(z,x) = k^2\psi_{\mathbf{k}}(z,x). \tag{A1}$$

Now from (48), $\psi_{\mathbf{k}}(\mathbf{r}) = e^{i\mathbf{k}\cdot\mathbf{r}} + \psi^s_{\mathbf{k}}(\mathbf{r})$, and we have seen that in II $\psi^s_{\mathbf{k}}(\mathbf{r})$ is a Bloch function along x with representation as in (56). Thus, in II, since a plane can be considered as a periodic function at the center of the first Brillouin zone, $\psi_{\mathbf{k}}(\mathbf{r})$ also can be treated as a Bloch function along x,

$$\psi_k(k_x,z,x) = \sum_{m=-\infty}^{\infty} U_{km}(k_x,z)e^{i(k_x+G_m)x}, \tag{A2a}$$

with

$$U_{km}(k_x,z) = e^{ik_z z}\delta_{m0} + U^s_{km}(k_x,z). \tag{A2b}$$

Then $U^r_{km}(k_x,0) = \delta_{m0} - U_{km}(k_x,0)$, once the $U_{km}(k_x,z)$ are known. Upon inserting (A2a) into (A1), and using the representation of $q(z,x)$ in (55a), we find after a few steps that

$$\sum_{m=-\infty}^{\infty} V_{km}(k_x,z)e^{iG_m x} = 0, \tag{A3a}$$

where, suppressing the k and k_x arguments,

$$V_m(z) = U''_m(z) + [k^2 - (k_x+G_m)^2]U_m(z) - \sum_n q_n(z)U_{m-n}(z). \tag{A3b}$$

Equation (A3a) formally defines a periodic function in x that vanishes everywhere. Therefore, we must have $V_m(z) = 0$ everywhere, giving us in region II a set of coupled one-dimensional equations, which, for $m = 0,\pm1,\pm2,\ldots$, can be written as

$$U''_m(z) + (\mathcal{E}_m - q_0)U_m(z) = Q_m(z), \tag{A4a}$$

where

$$\mathcal{E}_m(z) = k^2 - (k_x+G_m)^2 = k^2[1-(\cos\theta + m\tau)^2] \tag{A4b}$$

for incident $\angle\theta$ and with $\tau = \lambda/T_g$, as in (55b), and where

$$Q_m(z) = \sum_{n\neq m} q_{m-n}(z)U_n(z). \tag{A4c}$$

Let us here restrict attention to gratings composed of symmetric rectangular barriers of width w_g [with $q(z) = q \geqslant 0$ in the barrier and $q(z) = 0$ between barriers] and center the grating on $(x,z) = (x_g,0)$, where x_g is located at the center of a barrier; then we have

$$q_m = e^{-iG_m x_g}\tilde{q}_{|m|}, \tag{A5a}$$

with

$$\tilde{q}_m = \bar{q}\ \mathrm{sinc}\,\frac{G_m w_g}{2\pi} \tag{A5b}$$

and $\bar{q} = q w_g/T_g$. The "normalized" sinc function is

$$\mathrm{sinc}\,x = \frac{\sin\pi x}{\pi x},$$

so that $\mathrm{sinc}\,m = \delta_{m0}$. For these gratings,

$$Q_m(z) = \sum_{n\neq m} e^{-iG_{m-n}x_g}\tilde{q}_{|m-n|}U_n(z). \tag{A5c}$$

We see that $\tilde{q}_0 = q_0 = \bar{q}$ and that q_m is invariant under $x_g \to x_g + nT_g$.

Now $\psi_k(k_x,z,x)$ is subject to the continuity conditions,

$$\lim_{z\to 0^+} \nabla^{(j)}_{x,z}\psi_k(k_x,z,x) = \lim_{z\to 0^-} \nabla^{(j)}_{x,z}\psi_k(k_x,z,x), \tag{A6}$$

at $z = 0$ for the jth derivatives ($j = 0,1$). Taking (59) for $\psi_k(k_x,0^-,x)$ and (A2) for $\psi_k(k_x,0^+,x)$ gives

$$1 + r_0 = U_0(0), \quad ik_z(1 - r_0) = U_0'(0), \tag{A7a}$$

for $m = 0$, and

$$r_m = U_m(0), \quad -ik_z r_m = U_m'(0), \tag{A7b}$$

for $m \neq 0$. These conditions are summarized by

$$U_m^{(j)}(0) = (ik_z)^j[\delta_{m0} + (-1)^j r_m], \tag{A7c}$$

with $j = 0,1$. Similarly, at $z = L$,

$$U_m^{(j)}(L) = (ik_z)^j t_m, \tag{A7d}$$

where t_m is the transmission amplitude associated with scattering into $\mathbf{k}^t = (k_x + G_m)\hat{\mathbf{k}}_x + \hat{\mathbf{k}}_z k_z$. We note in passing that the Bloch form of the x dependence of $\psi_k(k_x,z,x)$ and $j = 0$ continuity are sufficient for $j = 1$ continuity in x at $z = 0$ and $z = L$.

The equations for $U_m(z)$ in (A4a) each have the form of an inhomogeneous Sturm-Liouville (S-L) problem,

$$L_m U_m(z) = Q_m(z), \tag{A8a}$$

with Liouville operator

$$L_m = \partial_z^2 + \mathcal{E}_m - q_0 \tag{A8b}$$

and "inhomogeneous" term $Q_m(z)$. This appearance is somewhat illusory in the usual S-L context, since the $Q_m(z)$ defined by (A4c), for $m = 0,\pm1,\pm2,\ldots$, cannot be specified independently of the desired $U_m(z)$ over the entire set of equations. Nevertheless, the analogy is useful for the purpose of generating a formal description of the solutions, which can serve as a starting point for controlled approximations. Thus, the set of solutions of (A8a) for $z \in$ II can be represented as

$$U_m(z) = U_m^c(z) + U_m^p(z), \tag{A9}$$

where $U_m^c(z)$ is the "complementary" solution of the homogeneous equation

$$L_m U_m^c(z) = 0 \tag{A10}$$

and $U_m^p(z)$ is the "particular" solution of (A8a), as if $U_m^c(z) \equiv 0$. We consider each of these in turn.

Notice that in a strict S-L problem, boundary conditions act only to fix the complementary solution. Here the continuity conditions of (A7) apply to the total solution. We impose specific conditions on the homogeneous problem shortly.

1. Complementary solution

Since $\mathcal{E}_m - q_0$ is independent of z, the solutions of the homogeneous problems (A10) are of the general form

$$U_m^c(z) = a_m^+ e^{i\kappa_m z} + a_m^- e^{-i\kappa_m z}, \tag{A11a}$$

with constants a_m^+ and a_m^- to be determined (see below), and where

$$\kappa_m = \sqrt{\mathcal{E}_m - q_0} = \sqrt{k_{zm}^2 - q_0}, \tag{A11b}$$

with

$$k_{zm} = \sqrt{k^2 - k_{xm}^2} \tag{A11c}$$

and

$$k_{xm} = k_x + G_m, \tag{A11d}$$

representing, respectively, the z and x components of an allowed reflected wave vector, such that $k_{xm}^2 + k_{zm}^2 = k^2$. So we can also write

$$\kappa_m = n_m k_{zm}, \tag{A11e}$$

where

$$n_m = \sqrt{1 - \frac{q_0}{k_{zm}^2}} \tag{A11f}$$

acts as an effective refractive index.

Now $k_{x0} = k_x$ and $k_{z0} = k_z$, so that $\kappa_0 = n_0 k_z$, with $n_0 = \sqrt{1 - q_0/k_z^2}$, as in the problem of specular reflection from a smooth, uniform film in region II with $q = q_0$. There are other useful ways of writing κ_m, so we also mention

$$\kappa_m = k\sqrt{1 - (\cos\theta + m\tau)^2 - \eta}, \tag{A12}$$

with $\eta = \bar{\rho}\lambda^2/\pi$.

Elastic scattering from the grating is allowed only if $\mathcal{E}_m \geqslant 0$, i.e., if k_{zm} is real valued. From (A4b), and always taking $k_x \geqslant 0$—i.e., $\pi/2 \geqslant \theta \geqslant 0$—we require $\cos\theta \leqslant 1 - m\tau$. This can not be satisfied for any $|m| \geqslant 1$ if $\tau > 1$ ($T_g < \lambda$); i.e., there is no off-specular reflection when the grating period is smaller than the neutron wavelength. For $\tau < 1$, the resulting restrictions are

$$m < \frac{1 - \cos\theta}{\tau} \tag{A13a}$$

at given θ or

$$\theta > \cos^{-1}(1 - m\tau) \tag{A13b}$$

for specified m. Therefore, for small-period gratings, i.e., periods comparable to a small number of wavelengths, we expect noticeably asymmetric off-specular reflection relative to the specular angle θ_0, with fewer observable peaks for $\theta > \theta_0$ than for $\theta < \theta_0$. On the other hand, for large-period gratings, i.e., when $\tau \ll 1$, we can expect more-or-less symmetrically disposed off-specular reflection.

The occurrence of $\kappa_m = 0$ can be called a *horizon*. Scattering involves a particular G_m only above its associated horizon, where κ_m is real valued. So for fixed τ and θ, the horizon is at $m = m_h = (1 - cos\theta)/\tau$, and no scattering occurs for $m > m_h$. While for fixed τ and m, the horizon is at $\theta = \theta_h = \cos^{-1}(1 - m\tau)$ and no scattering occurs for $\theta < \theta_h$. Above its horizon, $\kappa_m > 0$ by definition (for the given reflection geometry).

There remains the matter of determining the coefficient sets $\{a_m^\pm\}$. We address this after a discussion of the particular solution.

2. Particular solution

For any $Q_m(z)$, the particular solution $U_m^p(z)$ can always be generated by

$$U_m^p(z) = \int_0^L \mathcal{G}_m(z-z')Q_m(z')\,dz', \tag{A14a}$$

where $\mathcal{G}_m(z)$ is a Green's function of the Liouville operator L_m, satisfying

$$L_m\mathcal{G}_m(z) = \delta(z). \tag{A14b}$$

The Green's function appropriate to reflection from the slab geometry of our model film is

$$\mathcal{G}_m(z) = \frac{1}{2i\kappa_m}[e^{-i\kappa_m z}\Theta(-z) + e^{i\kappa_m z}\Theta(z)], \tag{A14c}$$

where $\Theta(z)$ is the Heaviside function,

$$\Theta(z) = \begin{cases} 1, & z > 0, \\ \frac{1}{2}, & z = 0, \\ 0, & z < 0. \end{cases}$$

The Green's function in (A14c) is verified to satisfy (A14b) using $\partial_z\Theta(z) = \delta(z)$.

It follows that, with a bit of manipulation,

$$U_m^p(z) = \frac{1}{2i\kappa_m}\sum_{n\neq m} e^{-iG_{m-n}x_g}\tilde{q}_{|m-n|} \times \left[e^{i\kappa_m z}\int_0^z e^{-i\kappa_m z'} + e^{-i\kappa_m z}\int_z^L e^{i\kappa_m z'}\right]U_n(z')\,dz', \tag{A15a}$$

which satisfies

$$\partial_z U_m^p(z) = \frac{1}{2}\sum_{n\neq m} e^{-iG_{m-n}x_g}\tilde{q}_{|m-n|} \times \left[e^{i\kappa_m z}\int_0^z e^{-i\kappa_m z'} - e^{-i\kappa_m z}\int_z^L e^{i\kappa_m z'}\right]U_n(z')\,dz'. \tag{A15b}$$

In particular,

$$\partial_z U_m^p(z)|_{z=0} = -i\kappa_m U_m(0) \tag{A16a}$$

and

$$\partial_z U_m^p(z)|_{z=L} = i\kappa_m U_m(L), \tag{A16b}$$

independently of the form of $U_m(z)$.

3. A solution ansatz

To get an idea of how this works, consider first the case that $\tilde{q}_{|m|} = 0$ for all $m \neq 0$. We expect, of course, that the resulting reflection is specular only, caused by a smooth, uniform film with $q = q_0$. Let us see in detail how this comes about. From (A4c) $Q_m(z) \equiv 0$, and we are left with the homogenous S-L problem (A10), with general solutions (A11a) and the continuity conditions at $z = 0$ in (A7c). Specifically, we have

$$\hat{U}_0''(z) + \kappa_0^2\hat{U}_0(z) = 0, \tag{A17a}$$

with continuity conditions $\hat{U}_0^{(j)}(0) = (ik_z)^j[1 + (-1)^j\hat{r}_0]$, for $j = 0,1$, while, for $m \neq 0$,

$$\hat{U}_m''(z) + \kappa_m^2\hat{U}_m(z) = 0, \tag{A17b}$$

with continuity conditions $\hat{U}_m^{(j)}(0) = (ik_z)^j(-1)^j\hat{r}_m$.

Here we employ the hat (ˆ) notation to identify the specular-only case. As in (A11), the general solution of (A17a) is

$$\hat{U}_0(z) = a_0^+e^{i\kappa_0 z} + a_0^-e^{-i\kappa_m z},$$

and from the continuity requirements at $z = 0$, one readily finds

$$\hat{a}_0^+ = \frac{1}{2}\left[1 + \hat{r}_0 + \frac{1}{n_0}(1-\hat{r}_0)\right], \qquad \hat{a}_0^- = \frac{1}{2}\left[1 + \hat{r}_0 - \frac{1}{n_0}(1-\hat{r}_0)\right], \tag{A18a}$$

so that

$$\hat{U}_0(z) = (1+\hat{r}_0)\cos\kappa_0 z + i(1-\hat{r}_0)\frac{\sin\kappa_0 z}{n_0}. \tag{A18b}$$

To get an explicit expression for $\hat{r}_0$, we also need to consider the continuity of $\hat{U}_0(z)$ at $z = L$, the boundary between regions II and III, which requires that $\hat{U}_0^{(j)}(L^-) = (ik_z)^j\hat{t}_0e^{ik_zL^+}$, for $j = 0,1$, where $\hat{t}_0$ is the transmission amplitude for the smooth, uniform film. Then with (A18b), we obtain two equations for the unknowns, $\hat{r}_0$ and $\hat{t}_0$, which, in particular, lead to

$$\hat{r}_0 = \frac{\left(n_0^{-1} - n_0\right)\sin\kappa_0 L}{\left(n_0^{-1} + n_0\right)\sin\kappa_0 L + 2i\cos\kappa_0 L} \quad \text{and} \qquad \hat{t}_0 = \frac{2e^{-ik_zL}}{\left(n_0^{-1} + n_0\right)\sin\kappa_0 L + 2i\cos\kappa_0 L}. \tag{A18c}$$

Thus is (A17) completely solved in terms of q_0 and k_z, with $\kappa_0 = \sqrt{k_z^2 - q_0} = n_0k_z$.

For $m \neq 0$ in (A17b), here repeated,

$$\hat{U}_m''(z) + \kappa_m\hat{U}_m(z) = 0,$$

with the continuity conditions $\hat{r}_m = \hat{U}_m(0^+) = \hat{a}_m^+ + \hat{a}_m^-$ and $-ik_z\hat{r}_m = \hat{U}_m'(0^+) = -i\kappa_m(\hat{a}_m^+ - \hat{a}_m^-)$. Physically, $\hat{r}_m = 0$, since the "grating" is completely smooth in x; so $\hat{a}_m = \hat{b}_m = 0$ at once for all $m \neq 0$. Alternatively, the continuity restraints on (A17b) can only be satisfied by a single wave emanating from the film into region I; but this cannot be a physical solution without a wave incident along $-z$ from region III, and there is no such wave in this problem.

In general, for all m we must solve

$$U_m(z) = a_m^+e^{i\kappa_m z} + a_m^-e^{-i\kappa_m z} + \sum_{n\neq m} e^{-iG_{m-n}x_g}\tilde{q}_{|m-n|} \times \int_0^L \mathcal{G}_{m-n}(z-z')U_n(z')\,dz', \tag{A19a}$$

subject to the continuity conditions at $z = 0$ and $z = L$,

$$U_m^{(j)}(0) = (ik_z)^j[\delta_{m0} + (-1)^j r_m], \tag{A19b}$$

and

$$U_m^{(j)}(L) = (ik_z)^j t_m. \tag{A19c}$$

Assume, for argument's sake, that M is the maximum relevant value of $|m|$. Then, in region I there are $2M+1$ reflection amplitudes to be determined, viz., $r_0, r_{\pm 1}, \ldots, r_{\pm M}$, and the $2(2M+1) = 4M+2$ associated continuity conditions in (A7c) at $z = 0$. Similarly, in III there are $2M+1$ transmission amplitudes, $t_0, t_{\pm 1}, \ldots, t_{\pm M}$ and the $4M+2$ associated conditions in (A7d) at $z = L$. Meanwhile, according to (A19), there are $2(2M+1)$ "free" variables associated with the complementary parts of the solutions, viz., $a_0^+, a_{\pm 1}^+, \ldots, a_{\pm M}^+$ and $a_0^-, a_{\pm 1}^-, \ldots, a_{\pm M}^-$. This means there are a total of $2(4M+2) = 8M+4$ equations from the combined continuity conditions at $z = 0$ and $z = L$ with which to determine the $8M+4$ variables $\{a_{\pm m}^{\pm}, r_{\pm m}, t_{\pm m}\}_{M+1}$.

The S-L problem specified by (A19) is self-consistent in the specific sense that the number of available boundary value equations matches the number of free variables to be determined, at least over a finite set of reciprocal lattice points $\{\pm m\}_{M+1}$ (i.e., if we throw away all $U_{\pm m}$ labeled by $|m| > M$). This is a necessary condition for unique solutions but also sufficient only if the system of equations is linearly independent. Linearity in the scattering amplitudes is obvious, since the continuity conditions are patently linear in $\{r_{\pm m}, t_{\pm m}\}_{M+1}$. Linearity in the complementary variables $\{a_{\pm m}^{\pm}\}_{M+1}$ may not obvious, but we can demonstrate it formally by iterating (A19a) on the complementary solution. Since this process quickly becomes unwieldy without some preparation, let us first write (A19) for any n_i (with $n_0 \equiv m$) as

$$U_{n_i}(z) = U_{n_i}^c(z) + \sum_{n_j \neq n_i} \mathcal{F}_{n_j}^{n_i} \star U_{n_j}(z), \tag{A20}$$

where $\star$ stands for convolution with respect to $z \in \{0, L\}$,

$$\mathcal{F}_{n_j}^{n_i} \star U_{n'}(z) = \int_0^L \mathcal{F}_{n_j}^{n_i}(z - z_j) U_{n_j}(z_j) dz_j \tag{A21}$$

and where

$$\mathcal{F}_{n_j}^{n_i}(z) = e^{-iG_{n_i - n_j} x_g} \tilde{q}_{|n_i - n_j|} \mathcal{G}_{n_i - n_j}(z). \tag{A22}$$

Then iteration of (A20), starting with $U_{n_0}(z) = U_{n_0}^c(z)$, gives

$$\begin{aligned} U_{n_0}(z) &= U_{n_0}^c(z) + \sum_{n_1 \neq n_0} \mathcal{F}_{n_1}^{n_0} \star U_{n_1}^c(z) \\ &\quad + \sum_{n_1 \neq n_0} \sum_{n_2 \neq n_1} \mathcal{F}_{n_1}^{n_0} \star \mathcal{F}_{n_2}^{n_1} \star U_{n_2}^c(z) + \cdots \\ &= U_{n_0}^c(z) + \sum_{N=1} \mathcal{V}_{n_0}^N(z), \end{aligned} \tag{A23a}$$

with

$$\begin{aligned} \mathcal{V}_{n_0}^N(z) &= \sum_{n_1 \neq n_0} \cdots \sum_{n_N \neq n_{N-1}} e^{-iG_{n_0 - n_N} x_g} \tilde{q}_{|n_0 - n_1|} \cdots \tilde{q}_{|n_{N-1} - n_N|} \\ &\quad \times \int_0^L \cdots \int_0^L dz_1 \cdots dz_N \mathcal{G}_{n_0 - n_1}(z - z_1) \cdots \\ &\quad \times \mathcal{G}_{n_{N-1} - n_N}(z_{N-1} - z_N) U_{n_N}^c(z_N). \end{aligned} \tag{A23b}$$

Thus, using (A11) for $U_{n_N}^c(z_N)$,

$$\begin{aligned} U_{n_0}(z) &= U_{n_0}^c + U_{n_0}^p \\ &= \sum_{N=0} \sum_{n_N} \left[\mathcal{W}_{n_0, n_N}^{N+}(z) a_{n_N}^+ + \mathcal{W}_{n_0, n_N}^{N-}(z) a_{n_N}^- \right], \end{aligned} \tag{A24}$$

where we have incorporated the homogeneous solution into the sum over N, defining

$$\mathcal{W}_{n_i, n_i}^{0,\sigma}(z) = e^{\sigma i \kappa_{n_i} z} \tag{A25a}$$

for $N = 0$, with $\sigma \equiv \pm 1$ and $i = 0, 1 \ldots$. Then, for $N > 0$,

$$\begin{aligned} \mathcal{W}_{n_0, n_1}^{1,\sigma}(z) &= (1 - \delta_{n_1 n_0}) e^{-iG_{n_0 - n_1} x_g} \tilde{q}_{|n_0 - n_1|} \\ &\quad \times \int_0^L \mathcal{G}_{n_0 - n_1}(z - z_1) e^{\pm i \kappa_{n_1} z_1} dz_1, \end{aligned} \tag{A25b}$$

$$\begin{aligned} \mathcal{W}_{n_0, n_2}^{2,\sigma}(z) &= e^{-iG_{n_0 - n_2} x_g} (1 - \delta_{n_1 n_0}) \sum_{n_1 \neq n_2} \tilde{q}_{|n_0 - n_1|} \tilde{q}_{|n_1 - n_2|} \\ &\quad \times \int_0^L \int_0^L dz_1 dz_2 \mathcal{G}_{n_0 - n_1}(z - z_1) \mathcal{G}_{n_1 - n_2}(z_1 - z_2) \\ &\quad \times e^{\sigma i \kappa_{n_2} z_2}, \end{aligned} \tag{A25c}$$

and so on. Notice that the summation restrictions in (A23b) apply only to adjacent indices, n_j, n_{j+1}; in (A25c), in particular, $n_2 = n_0$ is allowed but not $n_1 = n_0$. In general, for $N \geqslant 2$, closed "loops" in n_i occur if the associated weight $\tilde{q}_{|n_i - n_{i+1}|} \cdots \tilde{q}_{|n_{j+1} - n_i|} \neq 0$. For example,

$$\begin{aligned} U_0(z) &= \left[e^{i \kappa_{n_0} z} + \mathcal{W}_{0,0}^{2+}(z) + \cdots \right] a_0^+ \\ &\quad + \left[e^{-i \kappa_0 z} + \mathcal{W}_{0,0}^{2-}(z) + \cdots \right] a_0^- \\ &\quad + \left[\mathcal{W}_{0,-1}^{1+}(z) + \mathcal{W}_{0,-1}^{2+}(z) + \cdots \right] a_{-1}^+ \\ &\quad + \left[\mathcal{W}_{0,-1}^{1-}(z) + \mathcal{W}_{0,-1}^{2-}(z) + \cdots \right] a_{-1}^- \\ &\quad + \cdots. \end{aligned} \tag{A26}$$

The entire sequence started in (A25) can be notated as

$$\begin{aligned} \mathcal{W}_{n_0, n_N}^{N,\sigma}(z = z_0) &= e^{-iG_{n_0 - n_N} x_g} \left\{ \prod_{i=1}^N \sum_{n_{i-1}} \hat{q}_{|n_{i-1} - n_i|} \right\} \\ &\quad \times \prod_{i=1}^N \int_0^L dz_i \mathcal{G}_{n_{i-1} - n_i}(z_{i-1} - z_i) \mathcal{W}_{n_N, n_N}^{0,\sigma}(z_N) \end{aligned} \tag{A27}$$

for $N > 0$, where

$$\hat{q}_{|m-n|} \equiv (1 - \delta_{mn}) \tilde{q}_{|m-n|} \tag{A28}$$

succinctly incorporates the restriction to nonzero reciprocal lattice vectors and with $\sum_{n_0} \equiv 1$. To compute $\mathcal{W}_{n_0, n_N}^{N,\sigma}(z)$ in this form, we must integrate with respect to the z_i in the sequence $z_N, z_{N-1}, \ldots, z_1$.

With regard to the product symbol, we use the convention that $\prod_i f_i g = (\prod_i f_i) g$. Note also that

$$\left\{ \prod_{i=1}^N \sum_{n_{i-1}} \hat{q}_{|n_{i-1} - n_i|} \right\} \cdots$$

means

$$\begin{aligned} &\sum_{n_0} \sum_{n_1} \sum_{n_2} \cdots \sum_{n_{N-1}} \hat{q}_{|n_0 - n_1|} \hat{q}_{|n_1 - n_2|} \cdots \hat{q}_{|n_{N-1} - n_N|} \cdots \\ &\quad = \sum_{n_1} \sum_{n_2} \cdots \sum_{n_{N-1}} \hat{q}_{|n_0 - n_1|} \hat{q}_{|n_1 - n_2|} \cdots \hat{q}_{|n_{N-1} - n_N|} \cdots. \end{aligned}$$

4. Summary

For coding or other purposes, it may be helpful to summarize the solution ansatz, repeating some earlier equations. We are mostly concerned with obtaining the $4M+2$ reflection and transmission amplitudes $\{r_{\pm m}, t_{\pm m}\}_{M+1}$ for $0 \leqslant m \leqslant M$, where M labels the largest reciprocal lattice vectors that need to be considered for reasonably accurate solutions over a given angular range of measurement. The solution for these "physical" amplitudes also demands finding the $4M+2$ amplitudes $\{a^{\pm}_{\pm m}\}_{M+1}$ of the homogenous contributions to the wave function in the grating. All $8M+4$ variables are determined by the $8M+4$ linear equations obtained from the set

$$U_{n_0}(z) = \sum_{N=0} \sum_{n_N} \left[\mathcal{W}^{N+}_{n_0,n_N}(z) a^{+}_{n_N} + \mathcal{W}^{N-}_{n_0,n_N}(z) a^{-}_{n_N} \right], \quad \text{(A29)}$$

evaluated at $z=0$ and $z=L$ with the continuity conditions

$$U^{(j)}_m(0) = (ik_z)^j [\delta_{m0} + (-1)^j r_m] \quad \text{(A30a)}$$

and

$$U^{(j)}_m(L) = (ik_z)^j t_m \quad \text{(A30b)}$$

for $j=0$ [continuity of $U(z)$] and $j=1$ [continuity of $U'(z)$]. In (A29) the coefficients $\mathcal{W}^{N,\sigma}_{n_0,n_N}(z=0,L)$, with $\sigma = \pm$, are summarized by

$$\mathcal{W}^{N,\sigma}_{n_0,n_N}(z=z_0=0,L) = e^{-iG_{n_0-n_N}x_g} \left\{ \prod_{i=1}^{N} \sum_{n_{i-1}} \hat{q}_{|n_{i-1}-n_i|} \right\} \times \prod_{i=1}^{N} \int_0^L dz_i \mathcal{G}_{n_{i-1}-n_i}(z_{i-1}-z_i) \mathcal{W}^{0,\sigma}_{n_N,n_N}(z_N), \quad \text{(A31)}$$

independent of the solution variables. The z integrations in (A31) are defined by a Green's function for the slab geometry,

$$\mathcal{G}_m(z) = \frac{1}{2i\kappa_m} [e^{-i\kappa_m z}\Theta(-z) + e^{i\kappa_m z}\Theta(z)], \quad \text{(A32)}$$

with the grating substrate automatically incorporated into the κ variables, and by the initial condition

$$\mathcal{W}^{0,\sigma}_{n_i,n_i}(z) = e^{\sigma i \kappa_{n_i} z}. \quad \text{(A33)}$$

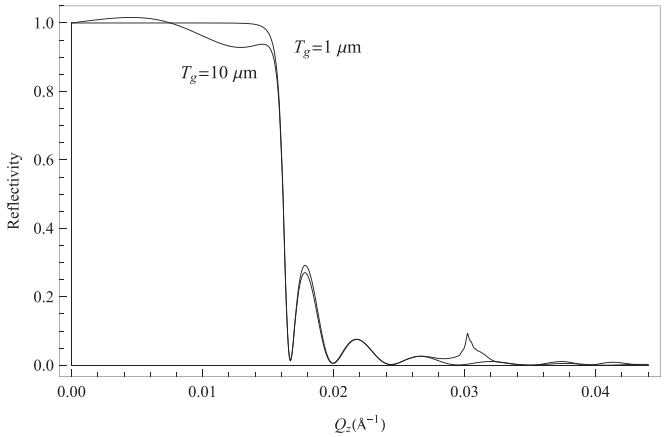

FIG. 7. Dynamic plane-wave specular reflectivity $|r_0|^2$ for two values of the grating period T_g. The grading linewidth is $w = 1/2\, T_g$, the line depth $L = 1000$ Å, grating material Ni, the substrate Si; the neutron wavelength is $\lambda = 4.75$ Å. $N=1$ ($\mathcal{W}$ linear in $\hat{q}$) in (A31). The maximum m value used is $M=8$, but $M \geqslant 1$ gives similar results at $Q_z \leqslant 0.02$. The curve for $T_g = 1$ μm virtually coincides with that for the averaged scattering length density of the grating over this Q_z range on a linear scale. The sharp feature near $Q_z = 0.03$ Å^{-1} for $T_g = 10$ μm is the first visible horizon effect; the slight rise above unity near $Q_z = 0$ is a computational artifact. [The linear equations obtained from (A29) and (A30) were solved using the "Solve" command of a commercial mathematical software package and were verified by direct matrix inversion.]

For m values over the horizon of the associated $r^{\pm}_m$ and $t^{\pm}_m$, the corresponding continuity equations must be eliminated. The number of equations to solve, therefore, is generally less than $8M+4$ at sufficiently large incident angles.

The summation over powers of $\hat{q}_{|n_{i-1}-n_i|}$ in (A31) may be suggestive of a distorted wave Born series. It is important to keep in mind, however, that the *solutions* of (A29) for the scattering amplitudes are not a power series in in the grating potential. Thus, even a truncated approximation of (A29) produces a fully dynamical result at small incident angles. Indeed, the terms in the series (A29) quickly become quite complicated with increasing N. However, for many purposes, even the first-order truncation at $N=1$ likely suffices at angles below all m horizons (see Fig. 3). Having said that, however, we acknowledge not having determined the formal behavior of the $\mathcal{W}$ series in (A29). An example of the specular reflectivity for a grating is shown in Fig. 7. A comparison with grating data for $T_g = 20$ μm, similar to the case $T_g = 10$ μm in the figure, is shown in Fig. 27 of Part I with some additional pertinent information.

[1] W. Zhu, Y. Huang, D. J. Kouri, M. Arnold, and D. K. Hoffman, Phys. Rev. Lett. **72**, 1310 (1994).

[2] C. F. Majkrzak, C. Metting, B. Maranville, J. Dura, S. Satija, and N. F. Berk, Phys. Rev. A **89**, 033851 (2014)..

[3] D. J. Tannor, *Introduction to Quantum Mechanics: A Time-dependent Perspective* (University Science Books, South Orange, NJ, 2007).

[4] M. Utsoro and V. K. Ignatovich, *Handbook of Neutron Optics* (Wiley-VCH, Wienheim, 2010).

[5] M. Tolan, W. Press, F. Brinkop, and J. P. Kotthaus, Phys. Rev. B **51**, 2239 (1995).

[6] R. Ashkar, P. Stonaha, A. Washington, V. R. Shah, M. R. Fitzsimmons, B. Maranville, C. F. Majkrzak, W. T. Lee, W. L. Schaich, and R. Pynn, J. Appl. Crystallogr. **43**, 455 (2010).

[7] L. E. Ballentine, *Quantum Mechanics: A Modern Development*, (World Scientific, Singapore, 1998).
[8] N. F. Berk and C. F. Majkrzak, Langmuir **25**, 4132 (2009).
[9] e.g., see *Beamline Geometry*, http://www.ncnr.nist.gov/reflpak/beam.html.
[10] M. Abramowitz and I. Stegun (editors), *Handbook of Mathematical Functions with Formulas, Graphs, and Mathematical Tables* (Dover, New York, 1972), online as NIST Digital Library of Mathemetical Functions, http://dlmf.nist.gov/